

# Geometric Entanglement and Quantum Phase Transition in Generalized Cluster-XY models

Aydin Deger<sup>1,2</sup> and Tzu-Chieh Wei<sup>1</sup>

<sup>1</sup>*C.N. Yang Institute for Theoretical Physics and Department of Physics and Astronomy,  
State University of New York at Stony Brook,  
Stony Brook, NY 11794-3840, USA*

<sup>2</sup>*Department of Applied Physics, Aalto University, 00076 Aalto, Finland*

(Dated: November 14, 2017)

## Abstract

In this work, we investigate quantum phase transition (QPT) in a generic family of spin chains using the geometric measure of entanglement (GE). In many of prior works, GE per site was used. Here, we also consider GE per block with each block size being two. This can be regarded as a coarse grain of GE per site. We introduce a useful parameterization for the family of spin chains that includes the XY models with  $n$ -site interaction, the GHZ-cluster model and a cluster-antiferromagnetic model, the last of which exhibits QPT between a symmetry-protected topological phase and an antiferromagnetic phase. As the models are exactly solvable, their ground-state wavefunctions can be obtained and thus their GE can be studied. It turns out that the overlap of the ground states with translationally invariant product states can be exactly calculated and hence the GE can be obtained via further parameter optimization. The QPTs exhibited in these models are studied and detected by the energy gap and singular behavior of geometric entanglement. In particular, the XzY model exhibits transitions from the nontrivial SPT phase to a trivial paramagnetic phase. Moreover, the halfway XY model exhibits a first-order transition across the Barouch-McCoy circle, on which it was only a crossover in the standard XY model. However, the halfway Ising model has no such transition.

PACS numbers: 03.65.Ud, 04.20.Jb, 05.30.Rt

## I. INTRODUCTION

Quantum entanglement has now been recognized as one of many intriguing consequences of quantum physics. It was nonetheless strongly objected by Einstein in his famous EPR paper [1]. Later, John Bell introduced inequalities that helped to gain more insight about quantum correlations [2] and motivated subsequent theoretical and experimental development [3–5]. These quantum correlations have since been verified many times in different experiments [4–7]. Quantum entanglement has also been found to provide resource for quantum information processing [8–12] and has been increasingly used as a tool for investigation in wide range of physics from quantum computation to black holes [13, 14]. There has been much work done for quantifying entanglement in many-body systems and many approaches have been developed to quantify entanglement in both bipartite and multipartite systems [15–17]. The entanglement entropy is perhaps the most well known example that measures quantum correlations between two halves of a pure quantum system [15]. Concurrence or the related entanglement of formation, as another example, quantifies entanglement between two qubits, and, among many useful features, there is an analytic formula for that [18]. For multipartite systems, there are various definitions but most of them are not easy to calculate [15]. Thus in this paper we will follow prior works and adopt a particular simple multipartite measure—the geometric measure of entanglement—to quantify entanglement for pure quantum systems and examine how it detects the quantum phase transitions for spin systems [19–21].

Phase transition is a phenomenon which describes change in the states of the matter due to control parameters such as temperature or pressure. Boiling of water or water freezing to ice is temperature-driven phase transitions that we experience in our daily life. On the other hand, quantum phase transition (QPT) [22] occurs at zero temperature, and, qualitatively speaking, it involves either level crossing or closing of an energy gap (between the ground and excited states) as the system size increases [22]. In the latter case, there is a diverging correlation length at the quantum critical point. The ground-state wavefunction there is expected to exhibit singular behavior, which can be characterized by how the entanglement changes near the critical point [23, 24]. Therefore, quantum entanglement may be an alternative way to detect quantum phase transition [15, 25], other than the thermodynamic quantities.

Since we are interested in systems at  $T = 0$ , we will be concerned with pure quantum many-body states,  $|\Psi\rangle$  of  $N$  spins, expressed in some local basis, as

$$|\Psi\rangle = \sum_{p_1 \dots p_N} \Psi_{p_1 p_2 \dots p_N} |e_{p_1}^{(1)} e_{p_2}^{(2)} \dots e_{p_N}^{(N)}\rangle. \quad (1)$$

A simple idea to quantify its quantum correlation is to see how close  $|\Psi\rangle$  can be approximated by uncorrelated product state  $|\Phi\rangle = \bigotimes_i |\phi^{[i]}\rangle$ , and thus the maximal overlap  $\Lambda_{\max}(\Psi) \equiv \max_{\phi's} |\langle \Phi | \Psi \rangle|$  is a quantity that measures such  $|\Psi\rangle$ 's closeness to product states. We can choose to use the form  $E_G(\Psi) \equiv -2 \log \Lambda_{\max}(\Psi)$ , which we call the geometric entanglement [19, 21], to quantify the quantum correlations in the state  $|\Psi\rangle$ . Moreover, in choosing different forms of product states  $|\Phi\rangle$ , one can probe different coarse-grained levels of entanglement, and these represent different hierarchies of quantum correlations:

$$\begin{aligned} |\Phi_1\rangle &= \bigotimes_i^N |\phi^{[i]}\rangle \Rightarrow \text{entanglement among all sites,} \\ |\Phi_2\rangle &= \bigotimes_i^{N/2} |\phi^{[2i-1, 2i]}\rangle \Rightarrow \text{entanglement among all blocks with 2 sites,} \\ |\Phi_L\rangle &= \bigotimes_i^{N/L} |\phi^{[Li-L-1, \dots, Li]}\rangle \Rightarrow \text{entanglement among all blocks of L sites.} \end{aligned}$$

In conforming with the intuitive picture of renormalization group (RG) on states (see e.g. Ref. [26]), we denote  $|\Psi'\rangle$  as the quantum state of  $|\Psi\rangle$  after one-step of RG via merging two sites into one, and the entanglement under such a RG procedure should therefore be defined as follows:

$$E(\text{RG}(\Psi)) = E(\{\Psi'\}) = \min_U E_1(\Psi'), \quad (2)$$

where the unitary  $U$  is of the form  $U[12] \otimes U[34] \otimes \dots \otimes U[2k-1, 2k] \otimes \dots$  and  $|\Psi'\rangle = U|\Psi\rangle$  denotes the unitary transformation that describes the merging (therefore acts on two neighboring sites in the original lattice). But since maximization over two-site unitary  $U[12]$  is equivalent to maximization over two-site state  $|\phi^{[12]}\rangle$ , we have that

$$\max_{\Phi_1} |\langle \Phi_1 | \Psi' \rangle| = \max_{\Phi_2} |\langle \Phi_2 | \Psi \rangle|, \quad (3)$$

and thus we see that the geometric entanglement w.r.t. to product of  $L$ -site states is the entanglement of RG after  $\log_2 L$  steps on the quantum state [27]. However, to calculate different hierarchies of entanglement is generally difficult. But as we see below, the first two

in the above, equivalently, the entanglement per site and per block of two, can be calculated for a wide class of exactly solvable spin chains.

The purpose of this paper is three-fold. Firstly, we describe and review the procedure for diagonalizing a large family of solvable spin chains which include the XY models with  $n$ -site interaction, the GHZ-cluster model and a cluster-antiferromagnetic model, the last of which exhibits QPT between a symmetry-protected topological phase and an antiferromagnetic phase. We provide a convenient parameterization of these and others, forming the family which we call the generalized cluster-XY models. In diagonalizing the Hamiltonians for finite sizes, we find and illustrate subtle points in getting the true ground state and the energy gap. Secondly, we show how to compute the geometric entanglement per site & per block of 2 sites for such systems and examine the quantum phase transition on the phase diagram. As explained above, this corresponds to the first two steps in the quantum-state RG procedure. One new ingredient here is the calculation of block entanglement per two sites. Thirdly, we hope that the various examples we include will be of use to readers interested in studying QPT from the perspective of entanglement. We provide both the energy gap and the entanglement for ground state, and use both of them for characterization of quantum phase transitions (if they exist) in various *cluster-XY models*. We shall see that the family of the models is interesting and displays many peculiar properties, as discussed below. Some of the models have been studied before in terms of entanglement, such as the standard XY model, the GHZ-cluster model by Wolf et al. [28], and the SPT-Antiferromagnetic model by Son et al. [29]. One new feature is that the three-site XY model (i.e. the XzY model) exhibits a transition from  $Z_2 \times Z_2$  SPT phase to a paramagnetic phase [30]. Moreover, among the family of the models, in the halfway XY model we find a first-order transition across the Barouch-McCoy circle, on which it was only a crossover for the standard XY model. However, the halfway Ising model has no such transition. In some of the models, the geometric entanglement displays a weak singularity, i.e., in the form of a cusp, and we can identify the point of singularity as states with infinite localizable entanglement.

The structure of this paper is as follows. In Sec. II, we introduce a parameterization of the generalized Hamiltonian for the cluster-XY model with  $n$ -site interaction. With this solution, one can diagonalize many bilinear Hamiltonian by substituting related parameters, quantify entanglement and detect quantum phase transition on the phase diagram. Then we give an illustrative example of Hamiltonian for XY model with  $n$ -site interaction using

our parameterization. In Sec. III, we introduce the geometric measure of entanglement per site and block for the multipartite many-body systems. We quantify global entanglement by calculating the overlap of ground-state wavefunctions and certain types of product states. The resultant entanglement will be used to examine quantum phase transitions in the family of the cluster-XY models. In Sec. IV, we study several examples such as XY model with three-site interaction and *halfway interaction*, whose geometric entanglement has not been analyzed before. The three-site interaction XzY model exhibits transitions from nontrivial SPT phase to a trivial paramagnetic phase. Moreover, the halfway XY model exhibits a first-order transition across the Barouch-McCoy arc, on which it is only a crossover in the standard XY model. However, the halfway Ising model has no such transition. Moreover, we present solutions of paramagnetic-ferromagnetic, GHZ-Cluster [27, 28], and symmetry-protected topological (SPT)-Antiferromagnetic [29] transitions by using this method. We make some concluding remarks in Sec. V.

## II. PARAMETERIZATION OF CLUSTER-XY MODELS WITH N-SITE INTERACTION

Quantum XY model was solved by Lieb, Schultz, Mattis in 1961 [31] and later all the statistical properties were examined by many other authors [32–39]. One of the most convenient ways to solve spin chain problems in one dimension is to describe the systems in bosonic or fermionic language. For example, one can analyze the Hamiltonian by using Holstein-Primakoff transformation [40] for mapping spin operators to bosonic annihilation and creation operators. On the other hand with the fermionic picture, Jordan-Wigner [41] and Bogoliubov transformations [42] provide a convenient way to diagonalize the Hamiltonians that are intrinsically free fermions.

Motivation of this section is to generalize one-dimensional bilinear Hamiltonians with XY interaction by introducing a parameterized Hamiltonian that describes a large family of quantum spin models whose ground state and geometric entanglement are exactly solved. Similar model has been discussed by Suzuki [43], but we provide a convenient parameterization that include further bilinear Hamiltonians. In particular, we introduce a few sets of parameters to describe the Hamiltonians, and diagonalize them to determine the energy spectrum. We also illustrate subtle points in determining the ground state and the energy

gap for finite systems.

### A. Parameterization of Hamiltonians and their diagonalization

We begin by defining the Hamiltonian for which there are a few types of parameters. We consider translational invariance and only models that are exactly solvable. The parameters  $N^{(x)}$  and  $N^{(y)}$  are the number of  $X$  and  $Y$  types of blocks in the Hamiltonian, respectively, and which represent  $X$  or  $Y$  interaction mediated by  $Z$ :  $X \underbrace{Z \dots Z}_{n^{(x)}} X$  or  $Y \underbrace{Z \dots Z}_{n^{(y)}} Y$ . We have indicated the numbers of consecutive  $Z$  sites for each block,  $n_l^{(x)}$  and  $n_{l'}^{(y)}$ , respectively. The subscript  $l$  ranges from 1 to  $N^{(x)}$  and  $l'$  from 1 to  $N^{(y)}$ . For example, one can build a Hamiltonian with three (e.g.  $N^{(x)} = 3$ )  $X$  interaction blocks, such as  $XX$ ,  $XZX$  and  $XZZX$ , and only one  $Y$ -type block ( $N^{(y)} = 1$ ), such as  $YZZZY$ . To indicate the strength of each block separately we use  $J_l^{(x)}$  and  $J_{l'}^{(y)}$ . For the above example, we have four such parameters,  $J_1^x$ ,  $J_2^x$ ,  $J_3^x$  and  $J_1^y$ . Finally,  $h$  is the strength of the transverse field. Thus the parameterized Hamiltonian reads:

$$H_{PXY} = - \sum_{j=1}^N \left( \sum_{l=1}^{N^{(x)}} J_l^{(x)} \sigma_{j-1}^x \sigma_j^z \dots \sigma_{j+n_l^{(x)}-1}^z \sigma_{j+n_l^{(x)}}^x + \sum_{l'=1}^{N^{(y)}} J_{l'}^{(y)} \sigma_{j-1}^y \sigma_j^z \dots \sigma_{j+n_{l'}^{(y)}-1}^z \sigma_{j+n_{l'}^{(y)}}^y + h \sigma_j^z \right). \quad (4)$$

where  $\sigma$ 's are the Pauli matrices associated with spin-1/2 angular momentum operators:

$$\sigma_j^x = \begin{pmatrix} 0 & 1 \\ 1 & 0 \end{pmatrix}, \quad \sigma_j^y = \begin{pmatrix} 0 & -i \\ i & 0 \end{pmatrix}, \quad \sigma_j^z = \begin{pmatrix} 1 & 0 \\ 0 & -1 \end{pmatrix},$$

and  $N$  indicate the system size. We remark that the family of models in this parameterization includes many interesting ones, such as the standard XY model and other interesting ones that have been explored from different perspectives [28, 29, 44].

Next, we will employ the Jordan-Wigner transformation, which realizes a spin to fermion mapping:

$$\sigma_i^x = \prod_{j=1}^{i-1} \left( 1 - 2c_j^\dagger c_j \right) \left( c_i + c_i^\dagger \right), \quad (5a)$$

$$\sigma_i^y = -i \prod_{j=1}^{i-1} \left( 1 - 2c_j^\dagger c_j \right) \left( c_i - c_i^\dagger \right), \quad (5b)$$

$$\sigma_i^z = 1 - 2c_i^\dagger c_i, \quad (5c)$$

where the fermionic creation and annihilation operators satisfy the canonical fermionic commutation relations  $\{c_i, c_j^\dagger\} = \delta_{ij}$ . To impose the periodic boundary conditions for spins, we rewrite the expression  $\sigma_N^x \sigma_{N+1}^x = \sigma_N^x \sigma_1^x$  as fermions:

$$\left(c_N + c_N^\dagger\right) \left(c_{N+1} + c_{N+1}^\dagger\right), \quad (6a)$$

$$= - \prod_{j=1}^N \left(1 - 2c_j^\dagger c_j\right) \left(c_N + c_N^\dagger\right) \left(c_1 + c_1^\dagger\right). \quad (6b)$$

One notices that there are two possibilities to hold the above equation. We define  $\mathcal{P} \equiv \prod_{j=1}^N \left(1 - 2c_j^\dagger c_j\right)$  as a parity operator with eigenvalues  $\pm 1$  depending on the total number of spins  $N$ . Since this operator commutes with Hamiltonian  $[H, \mathcal{P}] = 0$ , therefore, we can separate the Hamiltonian into two sector as even and odd,  $H = H^{(even)} + H^{(odd)}$ . The first sector (even) has the antiperiodic boundary condition for fermions but the total number of fermions is even,

$$\prod_{j=1}^N \left(1 - 2c_j^\dagger c_j\right) = 1, \quad c_{N+1} = -c_1. \quad (7a)$$

The other sector has periodic boundary condition where the total number of fermions is odd:

$$\prod_{j=1}^N \left(1 - 2c_j^\dagger c_j\right) = -1, \quad c_{N+1} = c_1. \quad (8a)$$

With the Jordan-Wigner transformation, we can rewrite the Hamiltonian in terms of the fermion operators as follows,

$$H_{PXY} = - \sum_{j=1}^N \left[ \sum_{l=1}^{N^{(x)}} J_l^{(x)} \left( c_{j-1}^\dagger c_{j+n_l^{(x)}} + c_{j-1}^\dagger c_{j+n_l^{(x)}}^\dagger - c_{j-1} c_{j+n_l^{(x)}} - c_{j-1} c_{j+n_l^{(x)}}^\dagger \right) + \sum_{l'=1}^{N^{(y)}} J_{l'}^{(y)} \left( c_{j-1}^\dagger c_{j+n_{l'}^{(y)}} - c_{j-1}^\dagger c_{j+n_{l'}^{(y)}}^\dagger + c_{j-1} c_{j+n_{l'}^{(y)}} - c_{j-1} c_{j+n_{l'}^{(y)}}^\dagger \right) + h(1 - 2c_j^\dagger c_j) \right]. \quad (9)$$

As the Hamiltonian is translationally invariant, we then perform a Fourier transformation, and we use a superscript  $(b)$  to indicate which of the two sectors:  $b = 0$  is for the periodic (odd sector) and  $b = 1/2$  the antiperiodic (even sector) boundary conditions,

$$c_j = \frac{1}{\sqrt{N}} \sum_{k=0}^{N-1} e^{i\frac{2\pi}{N}j(k+b)} \tilde{c}_k^{(b)}, \quad (10a)$$

$$\tilde{c}_k^{(b)} = \frac{1}{\sqrt{N}} \sum_{j=0}^{N-1} e^{-i\frac{2\pi}{N}j(k+b)} c_j. \quad (10b)$$

We then use the identities below (where  $x$  and  $y$  are integers indexing the sites and the notation  $\tilde{\phantom{c}}$  indicates the operator in the momentum space):

$$\sum_{j=1}^N c_{j+x} c_{j+y} = \sum_{k=0}^{N-1} e^{i\frac{2\pi}{N}[(x-y)(k+b)]} \tilde{c}_k \tilde{c}_{N-k-2b}, \quad (11a)$$

$$\sum_{j=1}^N c_{j+x}^\dagger c_{j+y}^\dagger = \sum_{k=0}^{N-1} e^{-i\frac{2\pi}{N}[(x-y)(k+b)]} \tilde{c}_k^\dagger \tilde{c}_{N-k-2b}^\dagger, \quad (11b)$$

$$\sum_{j=1}^N c_{j+x} c_{j+y}^\dagger = \sum_{k=0}^{N-1} e^{i\frac{2\pi}{N}[(x-y)(k+b)]} \tilde{c}_k \tilde{c}_k^\dagger. \quad (11c)$$

Substituting these into Eq. (9), we obtain the following form of the Hamiltonian,

$$\begin{aligned} H_{PXY} &= -Nh - \sum_{k=0}^{N-1} \left( \sum_l 2 J_l^{(x)} \cos \Theta_l^{(x)}(k) + \sum_{l'} 2 J_{l'}^{(y)} \cos \Theta_{l'}^{(y)}(k) - 2h \right) \tilde{c}_k^{(b)\dagger} \tilde{c}_k^{(b)} + \\ & i \left( \sum_l J_l^{(x)} \sin \Theta_l^{(x)}(k) - \sum_{l'} J_{l'}^{(y)} \sin \Theta_{l'}^{(y)}(k) \right) \left[ \tilde{c}_k^{(b)} \tilde{c}_{N-k-2b}^{(b)} + \tilde{c}_k^{(b)\dagger} \tilde{c}_{N-k-2b}^{(b)\dagger} \right], \\ & = -Nh + \sum_{k=0}^{N-1} \left[ 2\alpha_k \tilde{c}_k^{(b)\dagger} \tilde{c}_k^{(b)} - i\beta_k (\tilde{c}_k^{(b)} \tilde{c}_{N-k-2b}^{(b)} + \tilde{c}_k^{(b)\dagger} \tilde{c}_{N-k-2b}^{(b)\dagger}) \right] \quad (12) \end{aligned}$$

where we define for convenience  $\Theta$ 's,

$$\Theta_l^{(x)}(k, b) \equiv \frac{2\pi}{N}(k+b)(1+n_l^{(x)}), \quad (13a)$$

$$\Theta_{l'}^{(y)}(k, b) \equiv \frac{2\pi}{N}(k+b)(1+n_{l'}^{(y)}), \quad (13b)$$

and  $\alpha$ 's and  $\beta$ 's,

$$\beta_k^{(b)} = \sum_{l=1}^{N^{(x)}} J_l^{(x)} \sin \Theta_l^{(x)}(k, b) - \sum_{l'=1}^{N^{(y)}} J_{l'}^{(y)} \sin \Theta_{l'}^{(y)}(k, b), \quad (14a)$$

$$\alpha_k^{(b)} = h - \sum_{l=1}^{N^{(x)}} J_l^{(x)} \cos \Theta_l^{(x)}(k, b) - \sum_{l'=1}^{N^{(y)}} J_{l'}^{(y)} \cos \Theta_{l'}^{(y)}(k, b). \quad (14b)$$

We may sometimes suppress the argument ( $b$ ) in  $\Theta$  and the subscript ( $b$ ) in operators  $c$ 's,  $\alpha$ 's and  $\beta$ 's, when the context is clear.

To diagonalize this, we employ the Bogoliubov transformation that introduces mixing of

fermion creation and annihilation operators,

$$\tilde{c}_k = \cos \theta_k \gamma_k + i \sin \theta_k \gamma_{N-k-2b}^\dagger, \quad (15a)$$

$$\tilde{c}_{N-k-2b} = \cos \theta_k \gamma_{N-k-2b} - i \sin \theta_k \gamma_k^\dagger, \quad (15b)$$

$$\gamma_k = c_k \cos \theta_k - i \sin \theta_k c_{N-k-2b}^\dagger, \quad (15c)$$

$$\gamma_{N-k-2b} = c_{N-k-2b} \cos \theta_k + i \sin \theta_k c_k^\dagger, \quad (15d)$$

where the Bogoliubov fermions  $\gamma$ 's satisfy the same commutations:  $\{\gamma_i, \gamma_j^\dagger\} = \delta_{ij}$ . By choosing appropriate angles  $\theta_k$ 's, we can eliminate cross terms  $\gamma_k \gamma_{N-k-2b}$  and  $\gamma_k^\dagger \gamma_{N-k-2b}^\dagger$ , and obtain the diagonalized Hamiltonian:

$$H_{PXY} = \sum_{k=0}^{N-1} \epsilon_k \left( \gamma_k^\dagger \gamma_k - \frac{1}{2} \right), \quad (16)$$

where  $\epsilon_k$  is the single Bogoliubov particle's energy spectrum,

$$\epsilon_k = 2\sqrt{(\beta_k)^2 + (\alpha_k)^2}, \quad (17)$$

and the solution to  $\theta_k$ 's (which we also refer to as the Bogoliubov solution) is given by

$$\tan 2\theta_k = \frac{\beta_k}{\alpha_k}, \quad (18a)$$

$$\cos 2\theta_k = \frac{(\alpha_k)}{\sqrt{(\beta_k)^2 + (\alpha_k)^2}}, \quad (18b)$$

$$\sin \theta_k = \text{sgn}(\beta_k) \sqrt{\frac{1 - \cos 2\theta_k}{2}}. \quad (18c)$$

We emphasize a subtlety in obtaining the ground state and the gap. In order to obtain the true ground state, we have to compare the lowest energy in two sectors  $b = 0$  (periodic and odd fermions) and  $b = 1/2$  (antiperiodic and even fermions). A slight modification to the spectrum in Eq. (17) is when  $b = 0$  and  $k = 0$ , and in this case  $\Theta(k = 0) = 0$  and thus the  $k = 0$  component in the Hamiltonian (12) is already diagonal

$$\epsilon_{k=0}^{(b=0)} \tilde{c}_0^{(b=0)\dagger} \tilde{c}_0^{(b=0)} \equiv 2\alpha_{k=0}^{(b=0)} \tilde{c}_0^{(b=0)\dagger} \tilde{c}_0^{(b=0)}, \quad (19)$$

and thus  $\gamma_{k=0}^{(b=0)} = \tilde{c}_0^{(b=0)}$  (or equivalently  $\theta_{k=0}^{(b=0)} = 0$ ) and thus Eq. (17) for  $(k = 0, b = 0)$  is modified. Combining constant terms ( $Nh$  and others arising from the Jordan-Wigner transformation and commuting  $\gamma_k \gamma_k^\dagger = -\gamma_k^\dagger \gamma_k + 1$ ), the contribution from  $k = 0$  mode is then  $2\alpha_{k=0}^{(b=0)} (\tilde{c}_0^{(b=0)\dagger} \tilde{c}_0^{(b=0)} - 1/2)$ . Thus, the  $\epsilon_{k=0}^{(b=0)}$  should be taken as  $2\alpha_{k=0}^{(b=0)}$  in Eq. (17) above.

Moreover, when  $N$  is even,  $k$  can take the value  $k = N/2$ , and, similarly, the term in the Hamiltonian is also diagonal

$$\epsilon_{k=N/2}^{(b=0)} \tilde{c}_{N/2}^{(b=0)\dagger} \tilde{c}_{N/2}^{(b=0)} \equiv 2\alpha_{k=N/2}^{(b=0)} \tilde{c}_{N/2}^{(b=0)\dagger} \tilde{c}_{N/2}^{(b=0)}, \quad (20)$$

and thus  $\gamma_{k=N/2}^{(b=0)} = \tilde{c}_{k=N/2}^{(b=0)}$  or equivalently  $\theta_{k=N/2}^{(b=0)} = 0$  (when  $N$  is an even integer). The contribution of  $k = N/2$  mode to the Hamiltonian is thus  $2\alpha_{k=N/2}^{(b=0)} (\tilde{c}_{N/2}^{(b=0)\dagger} \tilde{c}_{N/2}^{(b=0)} - 1/2)$ . Therefore, when  $N$  is even, the  $\epsilon_{k=N/2}^{(b=0)}$  should be taken as  $2\alpha_{k=N/2}^{(b=0)}$  in Eq. (17) above.

In this  $b = 0$  sector, the total number of fermions should be odd, in order for the boundary condition Eq. (8) to be satisfied. For the number of total sites  $N$  being odd, because all excitation  $\epsilon_k \geq 0$  possibly except  $\epsilon_{k=0}$ , the lowest total energy in this sector has thus exactly one fermion. However, it is *not* necessarily the  $k = 0$  mode that is occupied, as when all  $\epsilon_k \geq 0$  (including the  $k = 0$  mode), it is possible that some other mode  $k \neq 0$  is the lowest, and it is thus energetically favorable to occupy this mode to achieve the lowest total energy, given the constraint of odd number of fermions. For  $N$  being even, the situation can be further complicated by the mode  $k = N/2$  with  $\epsilon_{k=N/2} = 2\alpha_{k=N/2}^{(b=0)}$ , which can be negative, and the ground state in this sector may have three fermions.

According to the above discussions, the associated lowest energy in  $b = 0$  sector for  $N$  even depends on where it is energetically favorable to occupy one or three fermions. In the case three fermions are occupied as the lowest energy state, it must involve  $\epsilon_{k=0}^{(b=0)} < 0$  and  $\epsilon_{(k=N/2)}^{(b=0)} < 0$ , as well as the lowest of the remaining modes, denoted by  $\epsilon_{k'}^{(b=0)}$  (but  $\geq 0$ ). They must satisfy the following condition that

$$\epsilon_{k=0}^{(b=0)} + \epsilon_{k=N/2}^{(b=0)} + \epsilon_{k'}^{(b=0)} < \min \left( \epsilon_{k=0}^{(b=0)}, \epsilon_{k=N/2}^{(b=0)} \right). \quad (21)$$

In this case, the lowest energy in this sector is

$$E_0^{(b=0, N \text{ even})} = \epsilon_{k=0}^{(b=0)} + \epsilon_{k=N/2}^{(b=0)} + \epsilon_{k'}^{(b=0)} - \frac{1}{2} \sum_{k=0}^{N-1} \epsilon_k^{(b=0)}, \quad (22)$$

and its associated wave function is

$$|\Psi^{(b=0)}\rangle \equiv \tilde{c}_0^{(0)\dagger} \tilde{c}_{k=N/2}^{(0)\dagger} \tilde{\gamma}_{k'}^{(b=0)\dagger} \prod_{k=1}^{k < \frac{N}{2}} \left[ \cos \theta_k^{(0)} + i \sin \theta_k^{(0)} \tilde{c}_k^{(0)\dagger} \tilde{c}_{N-k}^{(0)\dagger} \right] |\Omega\rangle. \quad (23)$$

Otherwise,

$$E_0^{(b=0, N \text{ even})} = \min_k \left( \epsilon_k^{(b=0)} \right) - \frac{1}{2} \sum_{k=0}^{N-1} \epsilon_k^{(b=0)}, \quad (24)$$

and the  $k^*$  that has the lowest  $\epsilon_{k^*}^{(b=0)}$  is often but not necessarily  $k = 0$  or  $k = N/2$ ; its associated wave function is

$$|\Psi^{(b=0)}\rangle \equiv \tilde{\gamma}_{k^*}^{(0)\dagger} \prod_{k=1}^{k < \frac{N}{2}} \left[ \cos \theta_k^{(0)} + i \sin \theta_k^{(0)} \tilde{c}_k^{(0)\dagger} \tilde{c}_{N-k}^{(0)\dagger} \right] |\Omega\rangle. \quad (25)$$

But as  $\epsilon_{N-k^*} = \epsilon_{k^*}$ , there is a degenerate wave function, by occupying  $k = N - k^*$  mode instead.

When  $N$  is odd, the lowest-energy state in this sector necessarily has one fermion, but it needs not be the  $k = 0$  mode. The total energy has a similar expression,

$$E_0^{(b=0, N \text{ odd})} = \min_k (\epsilon_k^{(b=0)}) - \frac{1}{2} \sum_{k=0}^{N-1} \epsilon_k^{(b=0)}. \quad (26)$$

Similarly, if the minimum  $\epsilon_k$  does not come from  $k = 0$ , then the energy is degenerate.

Let us move on to discuss the  $b = 1/2$  sector. In this sector, the total number of fermions should be even, in order for the boundary condition Eq. (7) to be satisfied. When  $N$  is odd, the fermion in the mode  $k = (N - 1)/2$  is not paired with any other, and the contribution to the Hamiltonian is thus  $2\alpha_{k=(N-1)/2} (\tilde{c}_{N/2}^{(b=1/2)\dagger} \tilde{c}_{(N-1)/2}^{(b=1/2)} - 1/2)$ . That is say that, when  $N$  is odd,  $\gamma_{k=(N-1)/2} = c_{k=(N-1)/2}$  or equivalently  $\theta_{k=(N-1)/2} = 0$ , and thus  $\epsilon_{k=(N-1)/2} \equiv 2\alpha_{k=(N-1)/2}$ . The lowest energy can arise in two scenarios. First, the simplest case is that there is no fermion. This occurs when

$$\epsilon_{k=(N-1)/2} + \min_{k \neq (N-1)/2} \epsilon_k \geq 0, \quad (27)$$

then

$$E_0^{(b=1/2), N \text{ odd}} = -\frac{1}{2} \sum_{k=0}^{N-1} \epsilon_k^{(b=1/2)}. \quad (28)$$

But if Eq. (27) is violated with optimal  $k'$  (and  $N - k' - 1$  as well), the ground-state energy in this sector is then degenerate and has the expression

$$E_0^{(b=1/2), N \text{ odd}} = \epsilon_{k=(N-1)/2} + \epsilon_{k'} - \frac{1}{2} \sum_{k=0}^{N-1} \epsilon_k^{(b=1/2)}. \quad (29)$$

However, there is no such modification when  $N$  is even. The lowest energy in the  $b = 1/2$  sector (with no  $\gamma$  fermions occupied) is thus,

$$E_0^{(b=1/2), N \text{ even}} = -\frac{1}{2} \sum_{k=0}^{N-1} \epsilon_k^{(b=1/2)}, \quad (30)$$

with the associated wavefunction being

$$|\Psi^{(b=1/2)}\rangle = \prod_{k=0}^{k < \frac{N-1}{2}} \left[ \cos \theta_k + i \sin \theta_k \tilde{c}_k^\dagger \tilde{c}_{N-k-1}^\dagger \right] |\Omega\rangle, \quad (31)$$

where we suppress the superscript ( $b = 1/2$ ) in  $\theta$ 's.

In order to determine the gap above the true ground state, we also need to find the next lowest energy in each sector, in addition to the lowest energies in both sectors  $E_0^{(b=1/2)}$  and  $E_0^{(b=0)}$ . It is *not* necessary that the gap is  $\Delta = |E_0^{(b=1/2)} - E_0^{(b=0)}|$ .

### B. Illustrative example: XY model with $n$ -site $Z$ -mediated interaction in the transverse field

In this part, we show how to choose parameters and thus obtain the solution of the XY model with  $n$ -site  $Z$  mediated XX and YY interaction. With this model one can grasp the general features of site-interactions by simply changing  $n$  value. For example, the standard XY model can be recovered by taking  $n = 0$ . Let us begin by listing the parameters that characterize this Hamiltonian:

$$N^{(x)} = 1, \quad N^{(y)} = 1, \quad (32a)$$

$$J_l^{(x)} = \{(1+r)/2\}, \quad J_l^{(y)} = \{(1-r)/2\}, \quad (32b)$$

$$n_l^{(x)} = \{n\}, \quad n_l^{(y)} = \{n\}. \quad (32c)$$

Substituting these parameters into Eq. (4), we obtain the corresponding Hamiltonian,

$$H_{XnY} = - \sum_{j=1}^N \left( \frac{1+r}{2} \sigma_{j-1}^x \sigma_j^z \cdots \sigma_{j+n-1}^z \sigma_{j+n}^x + \frac{1-r}{2} \sigma_{j-1}^y \sigma_j^z \cdots \sigma_{j+n-1}^z \sigma_{j+n}^y + h \sigma_j^z \right), \quad (33)$$

which can be diagonalized as

$$H = \sum_{k=0}^{N-1} \epsilon_k^{(b)} \left( \gamma_k^{(b)\dagger} \gamma_k^{(b)} - \frac{1}{2} \right), \quad (34)$$

$$\epsilon_k^{(b)} = 2 \sqrt{(r \sin \phi_k^n)^2 + (h - \cos \phi_k^n)^2}, \quad (35)$$

and Bogoliubov solution is as follows:

$$\tan 2\theta_k = \frac{r \sin \phi_k^n}{h - \cos \phi_k^n}, \quad (36)$$

where we define  $\phi_k$  for convenience

$$\phi_k^n \equiv \frac{2\pi}{N}(n+1)(k+b), \quad (37)$$

and  $n$  is the number of  $\sigma_z$  term in each  $X$  and  $Y$  blocks. The above spectrum  $\epsilon_k$ , of course, needs to be appropriately modified, for  $(k=0, b=0)$ ,  $(k=N/2, b=0)$ , and  $(k=(N-1)/2, b=1)$ , etc., as discussed previously. We note that by varying the number of  $\sigma_z$  one obtains other models:

$$\begin{aligned} n=0 & \rightarrow \text{XY model,} \\ n=1 & \rightarrow \text{XY model with three-site interaction}(H_{XzY}), \\ n=\frac{N}{2}-1 & \rightarrow \text{(for } N \text{ even) } \textit{halfway interaction.} \end{aligned}$$

We will investigate QPT for these models and others in sections below.

We can also build a different number of Z-mediated sites for each block, such as  $(n+2)$ -site interaction for  $X$  block and  $(m+2)$ -site interaction for  $Y$  block with the following parameters:

$$N^{(x)} = 1, \quad N^{(y)} = 1, \quad (38a)$$

$$J_l^{(x)} = \{(1+r)/2\}, \quad J_{l'}^{(y)} = \{(1-r)/2\}, \quad (38b)$$

$$n_l^{(x)} = \{n\}, \quad n_{l'}^{(y)} = \{m\}, \quad (38c)$$

and substituting parameters into  $H_{PXY}$  gives the following Hamiltonian:

$$H_{XnmY} = - \sum_{j=1}^N \left( \frac{1+r}{2} \sigma_{j-1}^x \sigma_j^z \cdots \sigma_{j+n-1}^z \sigma_{j+n}^x + \frac{1-r}{2} \sigma_{j-1}^y \sigma_j^z \cdots \sigma_{j+m-1}^z \sigma_{j+m}^y + h \sigma_j^z \right). \quad (39)$$

### III. GEOMETRIC MEASURE OF ENTANGLEMENT FOR GENERALIZED CLUSTER-XY MODELS

Entanglement has become a useful tool to study quantum criticality after several pioneering works on the behavior of entanglement near the quantum critical points [23, 25, 45–48]. Many of the previous works on entanglement investigated the domain of bi-partite systems. The geometric measurement of entanglement, introduced earlier, was based on a work of Barnum and co-workers [19] and developed further by Wei and collaborators [20, 21, 29, 49–51].

The main idea of analyzing entanglement is to find a minimum distance between the entangled state  $|\Psi\rangle$  and suitably defined product states, such as

$$|\Phi\rangle \equiv \bigotimes_{i=1}^n |\phi^{(i)}\rangle. \quad (40)$$

An essential quantity is the maximal overlap,

$$\Lambda_{\max}(\Psi) \equiv \max_{\Phi} |\langle \Phi | \Psi \rangle|, \quad (41)$$

from which we can define the geometric entanglement

$$E_G^{(1)}(\Psi) \equiv -\log_2 \Lambda_{\max}^2(\Psi), \quad (42)$$

and the entanglement density

$$\mathcal{E}^{(1)} \equiv \frac{E_{\log_2}(\Psi)}{N}, \quad (43)$$

where  $N$  denotes the total number of sites. We note that for GHZ states,  $\Lambda_{\max} = 1/2$  and thus  $E_G^{(1)} = 1$ . Similarly by properly defining the product state, we can define the geometric entanglement among blocks with each block containing 2 spins,  $E_G^{(2)}$  and its density  $\mathcal{E}^{(2)}$ , as discussed in the Introduction. In the following section, we present derivation of the overlaps for these two scenarios.

### A. Geometric Entanglement per site

Here, we review the derivation of the overlap of the ground state with a product state, comprised of product of single spin states:  $|\Phi_1\rangle = (a|\uparrow\rangle + b|\downarrow\rangle)^{\otimes N}$  which can be written as fermions by applying the Jordan-Wigner transformation

$$|\Phi_1\rangle = \bigotimes_{i=1}^N (a + b\sigma_i^-) |\uparrow\uparrow \dots \uparrow\rangle, \quad (44a)$$

$$= \prod_{i=1}^N \left[ a + b \prod_{j=1}^{i-1} (1 - 2c_j^\dagger c_j) c_i^\dagger \right] |\Omega\rangle, \quad (44b)$$

where  $|\Omega\rangle$  is the vacuum with no  $c$  fermions. Using this fact, we can further simplify the expression

$$|\Phi_1\rangle = \prod_{i=1}^N \left[ a + b c_i^\dagger \right] |\Omega\rangle = a^N \prod_{i=1}^N e^{b' c_i^\dagger} |\Omega\rangle, \quad (45)$$

$$= a^N e^{\sum_{i=1}^N b' c_i^\dagger} e^{\sum_{i<j} (b')^2 c_i^\dagger c_j^\dagger}, \quad (46)$$

where we have defined  $b' \equiv b/a$ . Note that  $e^A e^B = e^{A+B} e^{[A,B]/2} = e^{A+B} e^{AB}$  if  $A^2 = B^2 = 0$  and  $\{A, B\} = 0$ . For many such operators, we use  $e^{A_1} e^{A_2} \dots e^{A_k} = e^{\sum A_i} e^{\sum_{i < j} A_i A_j}$  to bring them to the same exponent. Namely,  $\prod_{i=1}^N e^{b' c_i^\dagger} = e^{\sum_{i=1}^N b' c_i^\dagger} e^{\sum_{i < j} (b')^2 c_i^\dagger c_j^\dagger}$ . Next, we need to express  $\sum_{i < j} c_i^\dagger c_j^\dagger$  in the momentum basis. Notice that we can relax the limit  $i < j$  in the sum to  $i \leq j$ , as  $c_i^\dagger c_i^\dagger = 0$ . For simplicity and for the purpose of illustration, we consider quantum XY model with nearest neighbor interaction with  $N$  being even, and consider the odd sector, i.e.,  $c_{j+N} = c_j$  and thus using the following Fourier transformation  $c_j = \frac{1}{\sqrt{N}} \sum_{k=0}^{N-1} e^{i \frac{2\pi}{N} j(k+1/2)} c_k$ , we calculate

$$\sum_{j \leq l} c_j^\dagger c_l^\dagger = \frac{1}{N} \sum_{j=1}^l \sum_{k, k'=0}^{N-1} e^{-i \frac{2\pi}{N} j(k+\frac{1}{2}) - i \frac{2\pi}{N} l(k'+\frac{1}{2})} c_k^\dagger c_{k'}^\dagger \quad (47a)$$

$$= \frac{1}{N} \sum_{k, k'=0}^{N-1} e^{-i \frac{2\pi}{N} (k+\frac{1}{2})} \frac{e^{-i \frac{2\pi}{N} l(k'+\frac{1}{2})} - e^{-i \frac{2\pi}{N} l(k+k'+1)}}{1 - e^{-i \frac{2\pi}{N} (k+\frac{1}{2})}} c_k^\dagger c_{k'}^\dagger. \quad (47b)$$

Noting that

$$\sum_{l=1}^N e^{-i \frac{2\pi}{N} l (k'+\frac{1}{2})} = e^{-i \frac{2\pi}{N} (k'+\frac{1}{2})} \frac{1 - e^{-i \frac{2\pi}{N} N(k'+\frac{1}{2})}}{1 - e^{-i \frac{2\pi}{N} (k'+\frac{1}{2})}} = \frac{e^{-i \frac{\pi}{N} (k'+\frac{1}{2})}}{i \sin \left[ \frac{\pi}{N} (k' + \frac{1}{2}) \right]}, \quad (48a)$$

$$\sum_{l=1}^N e^{-i \frac{2\pi}{N} l (k+k'+1)} = N \delta_{k+k'+1, N}, \quad (48b)$$

we arrive at

$$\sum_{j \leq l} c_j^\dagger c_l^\dagger = \frac{1}{N} \sum_{k, k'=0}^{N-1} \frac{e^{-i \frac{\pi}{N} (k+\frac{1}{2})}}{i \sin \left[ \frac{\pi}{N} (k + \frac{1}{2}) \right]} \frac{e^{-i \frac{\pi}{N} (k'+\frac{1}{2})}}{i \sin \left[ \frac{\pi}{N} (k' + \frac{1}{2}) \right]} c_k^\dagger c_{k'}^\dagger - \sum_{k=0}^{N-1} \frac{e^{-i \frac{\pi}{N} (k+\frac{1}{2})}}{i \sin \left[ \frac{\pi}{N} (k + \frac{1}{2}) \right]} c_k^\dagger c_{N-k-1}^\dagger. \quad (49)$$

The coefficient of the first term is symmetric in  $(k, k')$  and thus the sum makes no contribution, and we can symmetrize the second term, obtaining

$$\sum_{j \leq l} c_j^\dagger c_l^\dagger = \sum_{k=0}^{N-1} i \cot \left[ \frac{\pi}{N} (k + \frac{1}{2}) \right] c_k^\dagger c_{N-k-1}^\dagger. \quad (50)$$

Thus, we have rewritten  $|\Phi_1\rangle$  in terms of fermionic language,

$$|\Phi_1\rangle = a^N e^{\sum_{i=1}^N b' c_i^\dagger} e^{\sum_{i=1}^N (b')^2 \sum_{k=0}^{N-1} i \cot \left[ \frac{\pi}{N} (k+\frac{1}{2}) \right] c_k^\dagger c_{N-k-1}^\dagger} |\Omega\rangle, \quad (51)$$

and we can choose an arbitrary normalizable constants  $a = \cos \frac{\xi}{2}$  and  $b = \sin \frac{\xi}{2}$ . Note we assume the product state is also translation invariant.

In most cases in the thermodynamic limit, the ground state is in the sector of  $b = 1/2$  with no fermion, i.e.  $|\Psi_{1/2}\rangle$ . So we will calculate the overlap  $\langle\Phi_1|\Psi_{1/2}\rangle$  in order to obtain the entanglement for  $|\Psi_{1/2}\rangle$ . It is convenient to rewrite  $|\Phi_1\rangle$  in the similar pairing form as the ground state for the even  $N$  case,

$$|\Phi_1(\xi)\rangle = \prod_{k=0}^{k < \frac{N-1}{2}} \left( \cos^2 \frac{\xi}{2} + i \sin^2 \frac{\xi}{2} \cot \frac{\pi(k + \frac{1}{2})}{N} \tilde{c}_k^\dagger \tilde{c}_{N-k-1}^\dagger \right) |\Omega\rangle, \quad (52)$$

and thus we arrive at the overlap for even  $N$

$$\langle\Psi_{1/2}|\Phi(\xi)\rangle = \prod_{k=0}^{k < \frac{N-1}{2}} \left( \cos \theta_k \cos^2 \frac{\xi}{2} + \sin \theta_k \sin^2 \frac{\xi}{2} \cot \frac{\pi(k + \frac{1}{2})}{N} \right). \quad (53)$$

Maximizing  $\log_2 |\langle\Psi|\Phi\rangle|^2$  over  $\xi$ , we obtain the geometric entanglement Eq.(43) and the entanglement density.

One important point of the above calculations is that the product state can be expressed in terms of pair creations from the vacuum, in the same manner as the ground state. We shall see in the next section that for a different type of product states consisting of pairs of sites it is of the form of four-particle creations from the vacuum. Similar to this, the ground state will be conveniently re-expressed as creation of two corresponding pairs to match the structure.

## B. Geometric Entanglement per block

If we define the product state to be composed of tensor product of states for blocks of spins, we can investigate the geometric entanglement among these blocks as well as the entanglement per block. Each block can consist of  $L$  spins. For  $L = 2$ , we write product state, where coefficients  $a, b, c, d$  below are normalized but arbitrary constants.

$$|\phi^{[2i-1, 2i]}\rangle = a |\uparrow\rangle_{2i-1} \otimes |\uparrow\rangle_{2i} + b |\uparrow\rangle_{2i-1} \otimes |\downarrow\rangle_{2i} + c |\downarrow\rangle_{2i-1} \otimes |\uparrow\rangle_{2i} + d |\downarrow\rangle_{2i-1} \otimes |\downarrow\rangle_{2i}. \quad (54)$$

Using the Jordan-Wigner transformation, we can re-express the total product state  $|\Phi\rangle \equiv \otimes_{i=1}^{N/2} |\phi^{[2i-1, 2i]}\rangle$  as follows:

$$|\Phi\rangle = \bigotimes_{i=1}^{N/2} \left[ a + b \prod_{j=1}^{2i-1} (1 - 2c_j^\dagger c_j) c_{2i}^\dagger + c \prod_{j=1}^{2i-1} (1 - 2c_j^\dagger c_j) c_{2i-2}^\dagger + d c_{2i-1}^\dagger c_{2i}^\dagger \right] |\Omega\rangle, \quad (55)$$

where  $|\Omega\rangle$  is the vacuum with no  $c$  fermions, and we have assumed here that  $N$  is even. We note that we have introduced a parameter  $c$ , which should be clear to distinguish from the operators  $c$ 's (which carry a site index). Using the fact that the operators  $c$ 's annihilate the vacuum, we have

$$|\Phi\rangle = \bigotimes_{i=1}^{N/2} \left[ a + b c_{2i}^\dagger + c c_{2i-2}^\dagger + d c_{2i-1}^\dagger c_{2i}^\dagger \right] |\Omega\rangle \quad (56)$$

$$= a^{N/2} \left[ \bigotimes_{i=1}^{N/2} e^{b' c_{2i}^\dagger + c' c_{2i-1}^\dagger} \right] e^{d' \sum_{i=1}^{N/2} c_{2i-1}^\dagger c_{2i}^\dagger} |\Omega\rangle, \quad (57)$$

where we have defined  $b' \equiv b/a$ ,  $c' \equiv c/a$ , and  $d' \equiv d/a$ . Employing the trick used earlier to bring operators to the same exponent, we arrive at

$$|\Phi\rangle = a^{N/2} e^{\sum_{i=1}^{N/2} e^{b' c_{2i}^\dagger + c' c_{2i-1}^\dagger}} e^{\sum_{i<j} (e^{b' c_{2i}^\dagger + c' c_{2i-1}^\dagger})(e^{b' c_{2j}^\dagger + c' c_{2j-1}^\dagger})} e^{d' \sum_{i=1}^{N/2} c_{2i-1}^\dagger c_{2i}^\dagger} |\Omega\rangle. \quad (58)$$

As we also have the two lowest states  $|\Psi_b\rangle$  ( $b = 0, 1/2$ ) expressed in terms of fermionic basis, we can evaluate the overlap  $\langle\Psi_b|\Phi\rangle$  in a straightforward, though tedious manner. Note that in the sum  $\sum_{i<j}$ , we can safely put the limit as  $\sum_{i\leq j}$ , as when  $i = j$ , the term vanishes. Thus we need to evaluate  $\sum_{i\leq j}^{N/2} \left( c_{2i}^\dagger c_{2j}^\dagger, c_{2i-1}^\dagger c_{2j-1}^\dagger, c_{2i}^\dagger c_{2j-1}^\dagger, c_{2i-1}^\dagger c_{2j}^\dagger \right)$ , as well as  $\sum_i^{N/2} c_{2i-1}^\dagger c_{2i}^\dagger$  in terms of momentum sum. The calculations are as follows:

$$\sum_{i\leq j}^{N/2} \left( c_{2i-1}^\dagger c_{2j}^\dagger + c_{2i}^\dagger c_{2j-1}^\dagger \right) = -\frac{1}{2} \sum_{k_1, k_2=0}^{N-1} \frac{e^{i\frac{2\pi}{N}(k_1+\frac{1}{2})} + e^{i\frac{2\pi}{N}(k_2+\frac{1}{2})}}{1 - e^{-i\frac{2\pi}{N}2(k_1+\frac{1}{2})}} e^{-i\frac{2\pi}{N}2(k_1+\frac{1}{2})} (\dots) c_{k_1}^\dagger c_{k_2}^\dagger \quad (59)$$

$$\sum_{i\leq j}^{N/2} c_{2i}^\dagger c_{2j}^\dagger = -\frac{1}{2} \sum_{k_1, k_2=0}^{N-1} \frac{e^{-i\frac{2\pi}{N}2(k_1+\frac{1}{2})}}{1 - e^{-i\frac{2\pi}{N}2(k_1+\frac{1}{2})}} (\dots) c_{k_1}^\dagger c_{k_2}^\dagger \quad (60)$$

$$\sum_{i\leq j}^{N/2} c_{2i-1}^\dagger c_{2j-1}^\dagger = -\frac{1}{2} \sum_{k_1, k_2=0}^{N-1} \frac{e^{-i\frac{2\pi}{N}(k_1-k_2)}}{1 - e^{-i\frac{2\pi}{N}2(k_1+\frac{1}{2})}} (\dots) c_{k_1}^\dagger c_{k_2}^\dagger \quad (61)$$

$$\sum_{i\leq j}^{N/2} c_{2i-1}^\dagger c_{2i}^\dagger = \frac{1}{2} \sum_{k_1, k_2=0}^{N-1} e^{i\frac{2\pi}{N}(k_1+\frac{1}{2})} (\dots) c_{k_1}^\dagger c_{k_2}^\dagger, \quad (62)$$

where  $(\dots) \equiv (\delta_{k_1+k_2+1, N} + \delta_{k_1+k_2+1, N/2} + \delta_{k_1+k_2+1, 3N/2})$ . There are three Kronecker delta functions, the first of which,  $\delta_{k_1+k_2+1, N}$ , represents the same pairing  $(k, N - k - 1)$  as the ground state. The latter two,  $\delta_{k_1+k_2+1, N/2} + \delta_{k_1+k_2+1, 3N/2}$ , however, do not correspond to the same pairing, but instead correspond to terms broken from two pairs of  $(k, N - k - 1)$  to  $(k + N/2, N/2 - 1 - k)$  and  $(k + 3N/2, 3N/2 - 1 - k)$ .

We then collect those quadratic operators in the exponential of  $|\Phi\rangle$  in the following form

$$\hat{O} \equiv \sum_{k=0}^{k < (N/2-1)/2} \left( f_k c_k^\dagger c_{N-k-1}^\dagger - f_{N/2-1-k} c_{N/2+k}^\dagger c_{N/2-k-1}^\dagger + g_k c_k^\dagger c_{N/2-k-1}^\dagger + h_k c_{k+N/2}^\dagger c_{N-k-1}^\dagger \right). \quad (63)$$

This division of operators into four groups facilitates the calculation of the overlap. At last, the overlap reads:

$$\begin{aligned} \langle \Psi_{1/2} | \Phi \rangle = \chi_N \prod_{k=0}^{k < (N/2-1)/2} \left\{ a^2 \cos \theta_k \cos \theta_{\frac{N}{2}-k-1} + d^2 \sin \theta_k \sin \theta_{\frac{N}{2}-k-1} + \right. \\ \left. \cos \theta_{\frac{N}{2}-k-1} \sin \theta_k \left[ \frac{b^2 + c^2}{2} \cot \frac{2\pi}{N} \left( k + \frac{1}{2} \right) + b c \cot \frac{2\pi}{N} \left( k + \frac{1}{2} \right) \cos \frac{2\pi}{N} \left( k + \frac{1}{2} \right) \right. \right. \\ \left. \left. + a d \sin \frac{2\pi}{N} \left( k + \frac{1}{2} \right) \right] + \cos \theta_k \sin \theta_{\frac{N}{2}-k-1} \left[ - \frac{b^2 + c^2}{2} \cot \frac{2\pi}{N} \left( k + \frac{1}{2} \right) \right. \right. \\ \left. \left. + b c \cot \frac{2\pi}{N} \left( k + \frac{1}{2} \right) \cos \frac{2\pi}{N} \left( k + \frac{1}{2} \right) + a d \sin \frac{2\pi}{N} \left( k + \frac{1}{2} \right) \right] \right\}, \quad (64) \end{aligned}$$

with

$$\chi_N = 1 \text{ for } N/4 = \text{integer},$$

$$\chi_N = a \cos \theta_{\frac{1}{2}(\frac{N}{2}-1)} + d \sin \theta_{\frac{1}{2}(\frac{N}{2}-1)} \text{ for } N/2 = \text{odd integer}.$$

By maximizing  $\log_2 |\langle \Psi | \Phi \rangle|^2$  over parameters  $a, b, c, d$  we can obtain the entanglement per block. In the thermodynamic limit it is written as

$$\begin{aligned} \mathcal{E}_2 = - \max_{a,b,c,d} 4 \int_0^{\pi/2} d\mu \log_2 \left\{ a^2 \cos \theta(\mu) \cos \theta(\pi - \mu) + d^2 \sin \theta(\mu) \sin \theta(\pi - \mu) \right. \\ \left. + \sin[\theta(\mu) - \theta(\pi - \mu)] \frac{b^2 + c^2}{2} \cot \mu + \sin[\theta(\mu) + \theta(\pi - \mu)] \left[ b c \cot \mu \cos \mu + a d \sin \mu \right] \right\}. \quad (65) \end{aligned}$$

Here we assume the closest *product* state is product of identical two-spin state.

We note that the above expression will reduce to that for the single-site product states when we set the two-site state

$$a |\uparrow\uparrow\rangle + b |\uparrow\downarrow\rangle + c |\downarrow\uparrow\rangle + d |\downarrow\downarrow\rangle = (\alpha |\uparrow\rangle + \beta |\downarrow\rangle) (\alpha |\uparrow\rangle + \beta |\downarrow\rangle), \quad (66)$$

namely, we set  $a = \alpha^2$ ,  $b = c = \alpha\beta$ , and  $d = \beta^2$ . In the case of antiferromagnetic ground state, we can no longer assume the single-site product states to be translationally invariant.

However, in order to obtain the entanglement per site, we maximize the overlap  $\log_2 |\langle \Psi | \Phi \rangle|^2$  with following parameters:  $a = \alpha\gamma, b = \alpha\delta, c = \beta\gamma, d = \beta\delta$  where  $|\alpha|^2 + |\beta|^2 = |\gamma|^2 + |\delta|^2 = 1$ , which comes from a product state of two sites  $(\alpha |\uparrow\rangle + \beta |\downarrow\rangle)(\gamma |\uparrow\rangle + \delta |\downarrow\rangle)$ .

#### IV. EXAMPLES

After having introduced parameterized exact solution and calculated the overlap for entanglement of cluster-XY Hamiltonians, we examine a few examples.

##### A. The anisotropic XY model with three-site interaction (XzY model)

The first model analyzed using the geometric entanglement is the celebrated XY model, done in Ref. [21]. As a first example in our calculation, we present the solution of the anisotropic XY model with three-site interaction (XX and YY, each mediated by one-site Z term) in the transverse field and the ground-state entanglement. The similar Hamiltonian has been studied in triangular optical lattices [35–38]. The model in one dimension is exactly solvable. We find that near the critical point, the global entanglement shows divergence and QPT occurs between paramagnetic and ferromagnetic phases in the same way as in XY model in the transverse field, also consistent with the behavior of the energy gap. We introduce the following quantities that characterize the model:

$$N^{(x)} = 1, N^{(y)} = 1, \quad (67a)$$

$$J_l^{(x)} = \{(1+r)/2\}, J_{l'}^{(y)} = \{(1-r)/2\}, \quad (67b)$$

$$n_l^{(x)} = \{1\}, n_{l'}^{(y)} = \{1\}. \quad (67c)$$

Substituting these terms into  $H_{PXY}$  (4), we obtain the Hamiltonian for XY Model with three-site interaction (mediated by one-size  $\sigma^z$ ):

$$H_{XzY} = - \sum_{j=1}^N \left[ \frac{1+r}{2} \sigma_{j-1}^x \sigma_j^z \sigma_{j+1}^x + \frac{1-r}{2} \sigma_{j-1}^y \sigma_j^z \sigma_{j+1}^y + h \sigma_j^z \right], \quad (68)$$

where  $r$  is a magnetic anisotropy constant between  $\sigma_x$  and  $\sigma_y$  terms with  $0 \leq r \leq 1$ . When  $r = 1$  the model reduces the Ising model with nearest-neighbor interaction and in the limit  $r = 0$ , it becomes isotropic XY model with three-site interaction. Using Eq. (14) we

calculate  $\alpha_k$  and  $\beta_k$ ,

$$\beta_k = \left(\frac{1+r}{2}\right) \sin \Theta_l^{(x)} - \left(\frac{1-r}{2}\right) \sin \Theta_{l'}^{(y)}, \quad (69)$$

$$\alpha_k = h - \left(\frac{1+r}{2}\right) \cos \Theta_l^{(x)} - \left(\frac{1-r}{2}\right) \cos \Theta_{l'}^{(y)}, \quad (70)$$

with  $\Theta_1 = \Theta_1^{(x)} = \Theta_1^{(y)} = \frac{4\pi}{N}(k+b)$ . We then get the diagonalized Hamiltonian and exact energy spectrum (See Eq. 16-20):

$$H = \sum_{k=0}^{N-1} \epsilon_k^{(b)} \left( \gamma_k^{(b)\dagger} \gamma_k^{(b)} - \frac{1}{2} \right). \quad (71)$$

The eigenvalues can be obtained by carefully analyzing odd sector ( $b = 0$ , periodic boundary conditions) and even sector ( $b = 1/2$ , antiperiodic boundary conditions) separately, assuming  $N$  is even:

$$\epsilon_k^{(b)} = \left\{ \begin{array}{ll} 2(h-1), & \text{for } k=0 \wedge b=0 \\ 2(h-1), & \text{for } k=\frac{N}{2} \wedge b=0 \\ 2(h-1), & \text{for } k=\frac{N-1}{2} \wedge b=1/2 \end{array} \right\} = 2\alpha_k^{(b)}, \quad (72)$$

or otherwise:

$$\epsilon_k^{(b)} = 2\sqrt{(\beta_k)^2 + (\alpha_k)^2} = 2\sqrt{\left(r \sin \frac{4\pi}{N}(k+b)\right)^2 + \left(h - \cos \frac{4\pi}{N}(k+b)\right)^2}, \quad (73)$$

with the corresponding Bogoliubov solution:

$$\tan 2\theta_k^{(b)} = \frac{\beta_k}{\alpha_k} = \frac{r \sin \Theta_1}{h - \cos \Theta_1}. \quad (74)$$

One notices that, the solution is very similar to the solution of the standard XY model [31, 39, 52]. The only difference occurs in the momentum space by a factor of two, i.e., in the XY model  $\Theta_1$  is  $2\pi(k+b)/N$  instead of  $4\pi(k+b)/N$ . But there are some differences that are related to the subtlety in getting the global lowest energy state. For example, in the XY model with  $r \neq 1$ , the state of the lowest energy can come from either the even or the odd sector, as illustrated in Fig. 1b for  $r = 0.5$ . As a function of  $h$ , the ground state switches between the two sectors, as the lowest energy changes between  $E_0^{(b=0)}$  and  $E_0^{(b=1/2)}$ . But for the XzY model, the ground state is always in the even sector with zero fermion, as illustrated in Fig. 1a. Moreover, for the odd-number fermion case ( $b = 0$ ), the lowest-energy level in this sector depends on the control parameter ( $h$ ) and anisotropy constant ( $r$ ). For

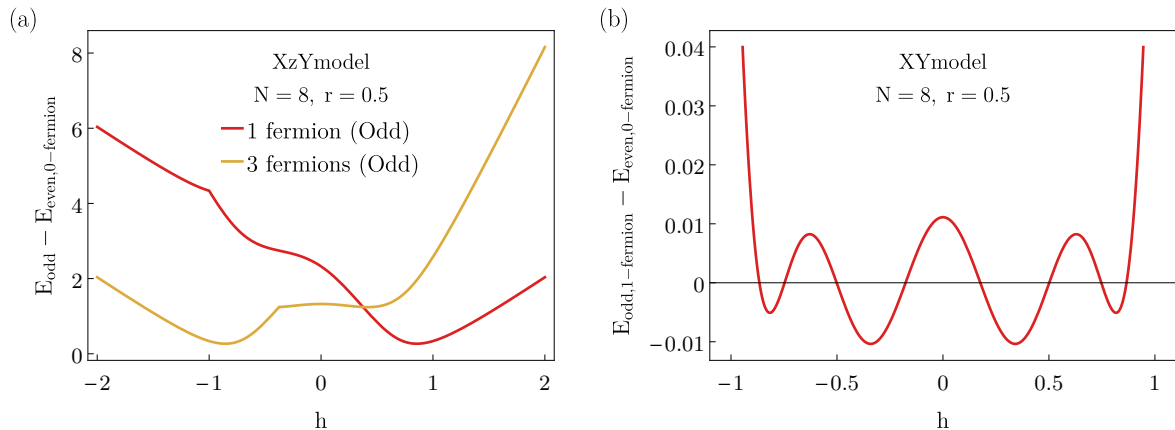


FIG. 1: The energy difference:  $E_{\text{odd}} - E_{\text{even}}$ , where  $E_{\text{odd}}$  is the lowest energy in the odd sector and  $E_{\text{even}}$  is that in the even sector. (a) For the XzY model with  $r = 0.5$  and  $N = 8$ . It is seen that the ground-state energy is always  $E_{\text{even}}$ , from the even sector. (b) For XY model with  $r = 0.5$  and  $N = 8$ . In contrast, it is seen that the ground state switches back and forth between the even and odd sectors, depending on the value of  $h$ .

example, in the Ising limit where  $r = 1$ , the odd sector has three-fermion occupation as the lowest-energy state in the region of  $h < 0$ ; otherwise it is energetically favorable to occupy one fermion for even  $N$ ; see Fig. 2(a) and also Fig. 1a. (But the true ground state arises from the  $b = 1/2$  (even) sector and has no  $\gamma$  fermion.) This phenomenon differs from the standard XY model where the lowest energy in the odd sector always has one-fermion occupation. The possibility of such peculiarity was discussed in the Sec. II A; see discussions around Eq. (21). We note that for a finite system size  $N$ (even) and  $r = 0.5$ , the lowest-energy level in the odd sector has three fermions from negative  $h$  values up to about  $h \approx 0.4$ ; see Fig. 3(a) and Fig. 1a. Moreover, the energy gap between the ground and first excited state is closing with an increasing system size  $N$  at  $h = 1$ , implying a quantum phase transition there; see Fig. 3(b) & Fig. 2(b) and note that, for small finite sizes, the gap as a function of  $h$  is not smooth for  $r = 0.5$ . In contrast, the gap vs.  $h$  is smooth for  $r = 1$  even with finite sizes, and in the thermodynamic limit  $N \rightarrow \infty$ , the energy gap for  $r = 1$  (Ising limit of XzY model) becomes  $2|1 - |h||$ .

To examine the quantum phase transition in the phase diagram, we also calculate geometric entanglement by substituting Bogoliubov solution into Eq. (43) and Eq. (53). We show the entanglement per site in Fig. 4 over a wide range of  $r$  and  $h$ . It is clearly seen

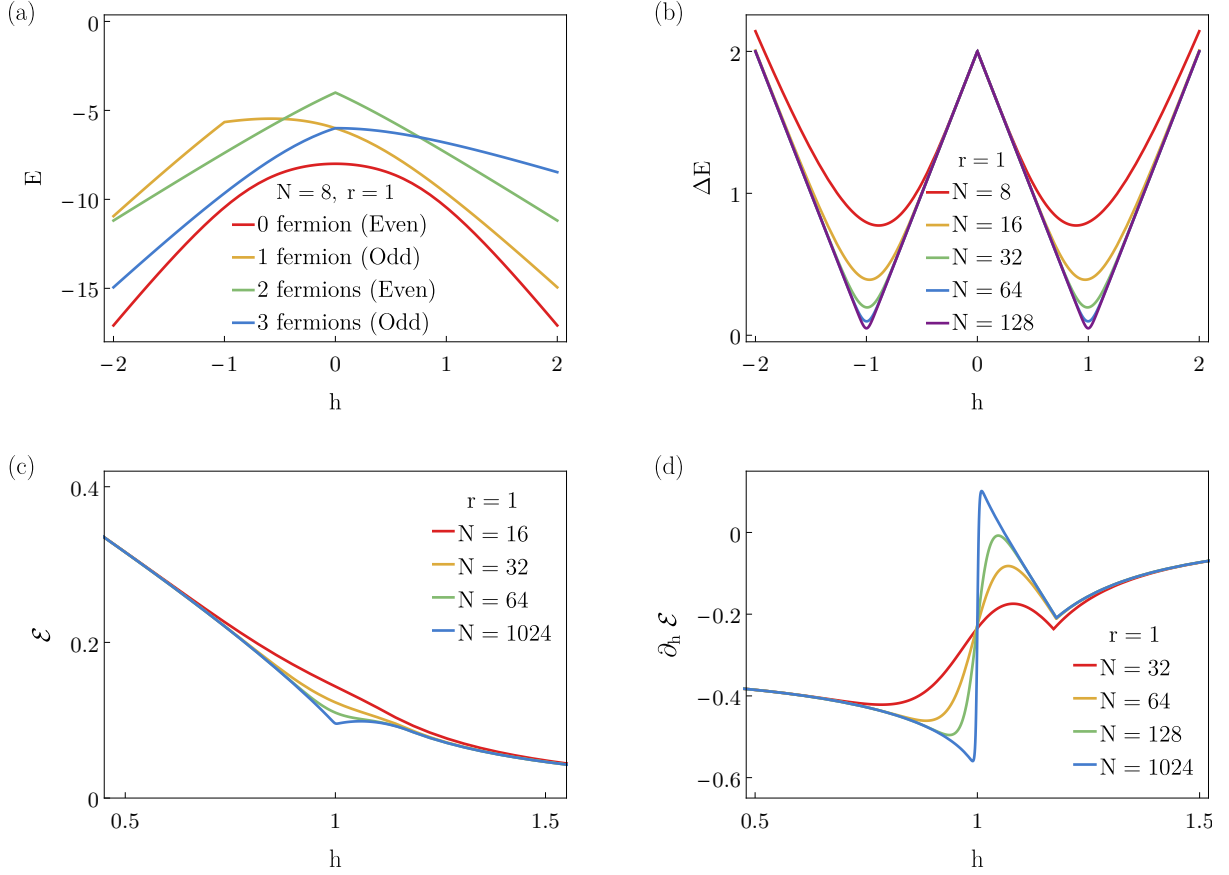


FIG. 2: (a) Lowest few energy levels vs.  $h$  for the XzY model with an anisotropy  $r = 1$  and the system size  $N = 8$ . The model essentially becomes the Ising model with next-nearest neighbor interaction (except the mediating  $Z$  factor) in the transverse field. In the odd sector, lowest one-fermion and three-fermions energy levels intercept at  $h = 0$ . The red line indicates the ground state comes from even sector with zero fermion occupation. (b) The energy difference between the ground and first excited states as a function of  $h$  at  $r = 0.5$ . At the critical point  $h = 1$ , the energy gap is closing as a function of the system size, which indicates a second-order quantum phase transition. In the thermodynamic limit ( $N \rightarrow \infty$ ), the energy gap becomes  $2|1 - |h||$ . (c) Quantum entanglement of XzY model with the anisotropy  $r = 1$  and with increasing system sizes  $N = 32, 64, 128, 1024$ . (d) The derivative of the entanglement density of XzY model for  $r = 1$ . The derivative of entanglement diverges and the QPT occurs at  $h = 1$  between a nontrivial SPT phase for  $h < 1$  and a trivial paramagnetic phase for  $h > 1$ .

that the behavior is singular across  $h = 1$ , similar to that in the standard XY model [21]. We illustrate this for two different  $r$ 's ( $r = 0.5$  &  $r = 1$ ) in Fig. 3(c) & Fig. 2(c), as well

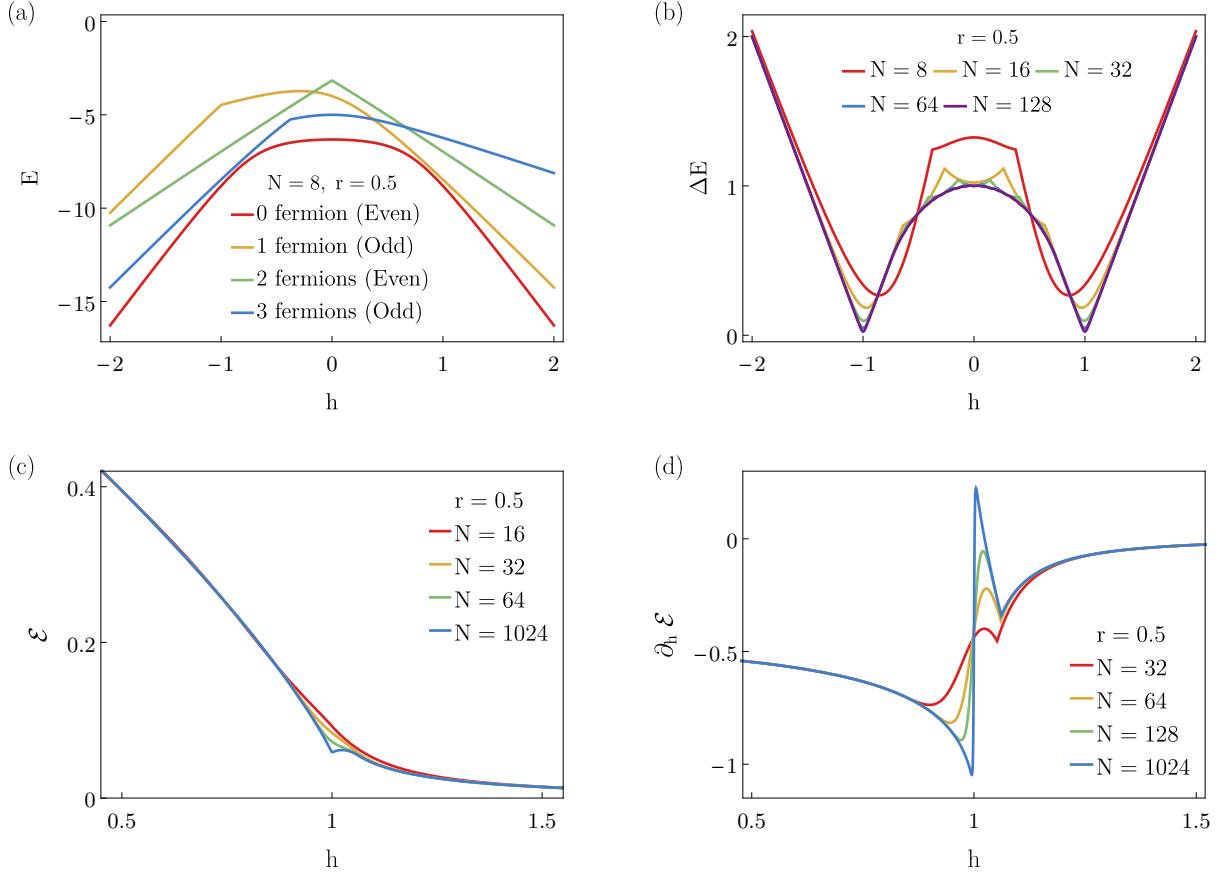


FIG. 3: (a) Lowest few energy levels vs.  $h$  for the XzY model with an anisotropy  $r = 0.5$  and the system size  $N = 8$ . In the specific region ( $h \lesssim 0.5$ ), the first excited state has three-fermion occupation, which is energetically favorable than one-fermion occupation. The possibility of this peculiarity has been discussed in Eq. (21). However, the red line shows that the ground state energy comes from even sector with zero fermion occupation. (b) The energy difference of the ground and first excited states as a function of  $h$  at  $r = 0.5$ . At the critical point  $h = 1$ , the energy gap is closing as a function of the system size, which indicates a second order quantum phase transition. (c) Quantum entanglement of XY model with three-site interaction in the transverse field (also labeled as the XzY model), where the anisotropy  $r = 0.5$  with increasing system sizes  $N = 32, 64, 128, 1024$ . (d) The derivative of entanglement density of XzY model for  $r = 0.5$ . The derivative of entanglement diverges and the QPT occurs at  $h = 1$  between a nontrivial SPT phase for  $h < 1$  and a trivial paramagnetic phase for  $h > 1$ .

as the entanglement derivative w.r.t.  $h$  in Fig. 3(d) & Fig. 2(d). The derivative of the entanglement develops singularity which indicates a quantum phase transition.

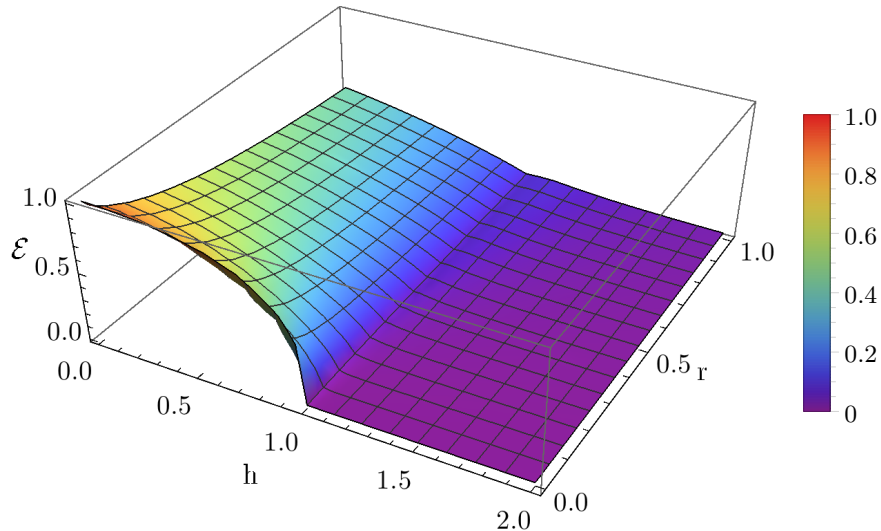


FIG. 4: Entanglement density per site vs transverse magnetic field ( $h$ ) vs anisotropy ( $r$ ) for XzY model with  $N = 1000$  spins.

We note that for  $r = 1$  the Hamiltonian reduces to

$$H = - \sum_j (\sigma_{j-1}^x \sigma_j^z \sigma_{j+1}^x + h \sigma_j^z). \quad (75)$$

The model has a  $Z_2 \times Z_2$  symmetry, generated by  $U_e = \prod_{j \text{ even}} \sigma_j^z$  and  $U_o = \prod_{j \text{ odd}} \sigma_j^z$  [30]. At  $h = 0$ , the ground state is known to be the cluster state, which is a nontrivial SPT state. (One expects this nontrivial SPT order to hold for general  $n$ -site mediated Ising model with  $Z_2^{\otimes n+1}$  symmetry; see Ref. [44].) At large  $h$ , the ground state is a trivial paramagnetic state. As we have seen that there is a quantum phase transition at  $h = 1$ , detected by the gap closing and the entanglement singularity. In fact, the XzY model Eq. (68) at any  $r$  has the  $Z_2 \times Z_2$  symmetry, and we expect that for  $0 < r \leq 1$ , the phase diagram contains a nontrivial SPT phase for  $h < 1$  (as there is no phase transition inside that region) and a trivial paramagnetic phase for  $h > 1$ , separated at a critical line at  $h = 1$ . This compares to the standard XY model, where  $h = 1$  separates a ferromagnetic phase from a paramagnetic phase. We also expect that this is a generic behavior for general  $n$ ; see also Ref. [44].

## B. XY model with halfway interaction

In the section II B, we have introduced an illustrative example of XY model with  $n$ -site  $Z$ -mediated XX and YY interactions. For  $n = 0$  and  $n = 1$ , we recover the standard

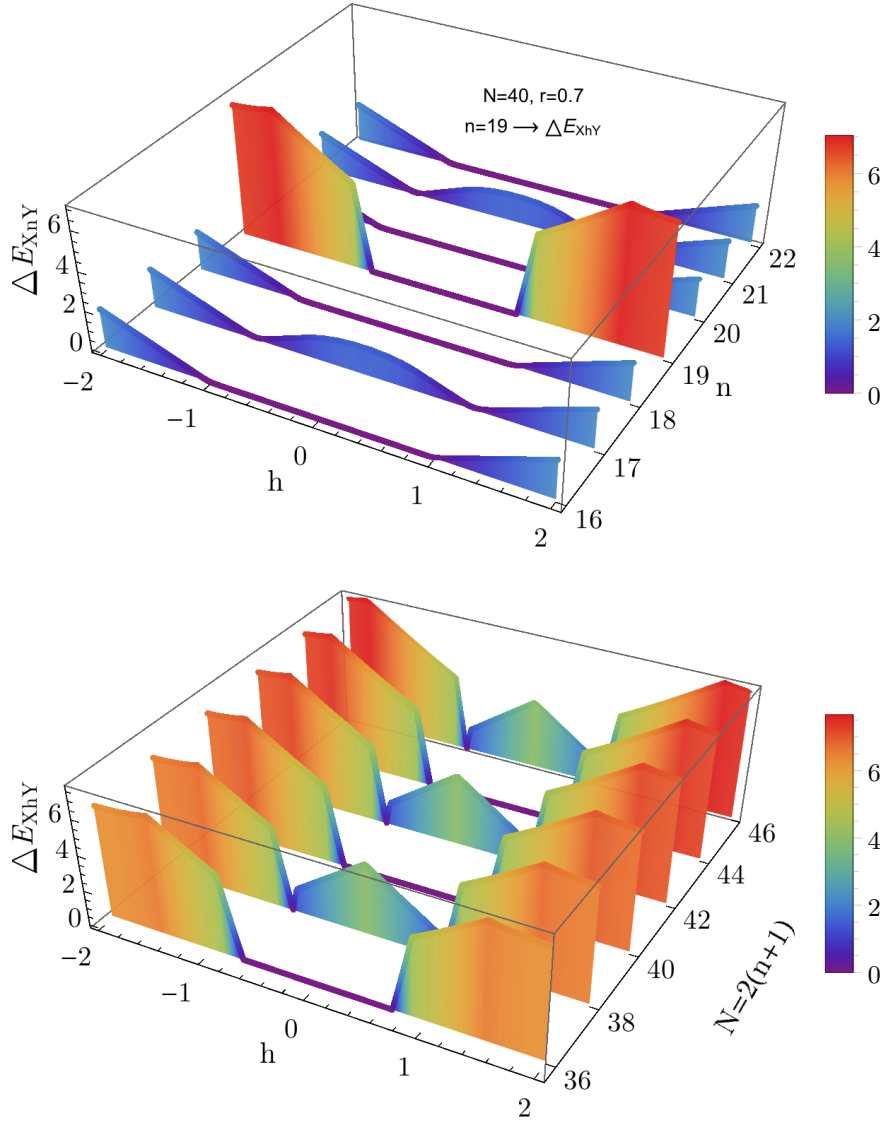


FIG. 5: (a) The upper figure illustrates the energy gap for XnY model (namely, XY model with  $n$ -site Z mediated interaction) with the anisotropy  $r = 0.7$  at a fixed system size  $N = 40$  vs. the mediating Z number ( $n$ ) between 16-22 and vs. the transverse magnetic field  $h$ . We notice a jump in the energy gap at  $\sqrt{1-r^2} \approx 0.714$  for the halfway XY model ( $n = N/2 - 1 = 19$ ). (b) The lower figure illustrate the energy gap for the halfway XY model (denoted by XhY) with the following parameters:  $N^{(x)} = N^{(y)} = 1$ ,  $J_l^{(x)} = \{(1+r)/2\}$ ,  $J_l^{(y)} = \{(1-r)/2\}$ ,  $n_l^{(x)} = n_l^{(y)} = \{N/2 - 1\}$ . The energy gap has different characteristics between  $N = 4m$  and  $N = 2(2m + 1)$ , as the former is degenerate and the latter is gapped in the region  $|h| < \sqrt{1-r^2}$ .

XY model and the XY model with three-site interaction (XzY model) investigated in the previous example. In this part, we demonstrate how a specific choice of site interaction,

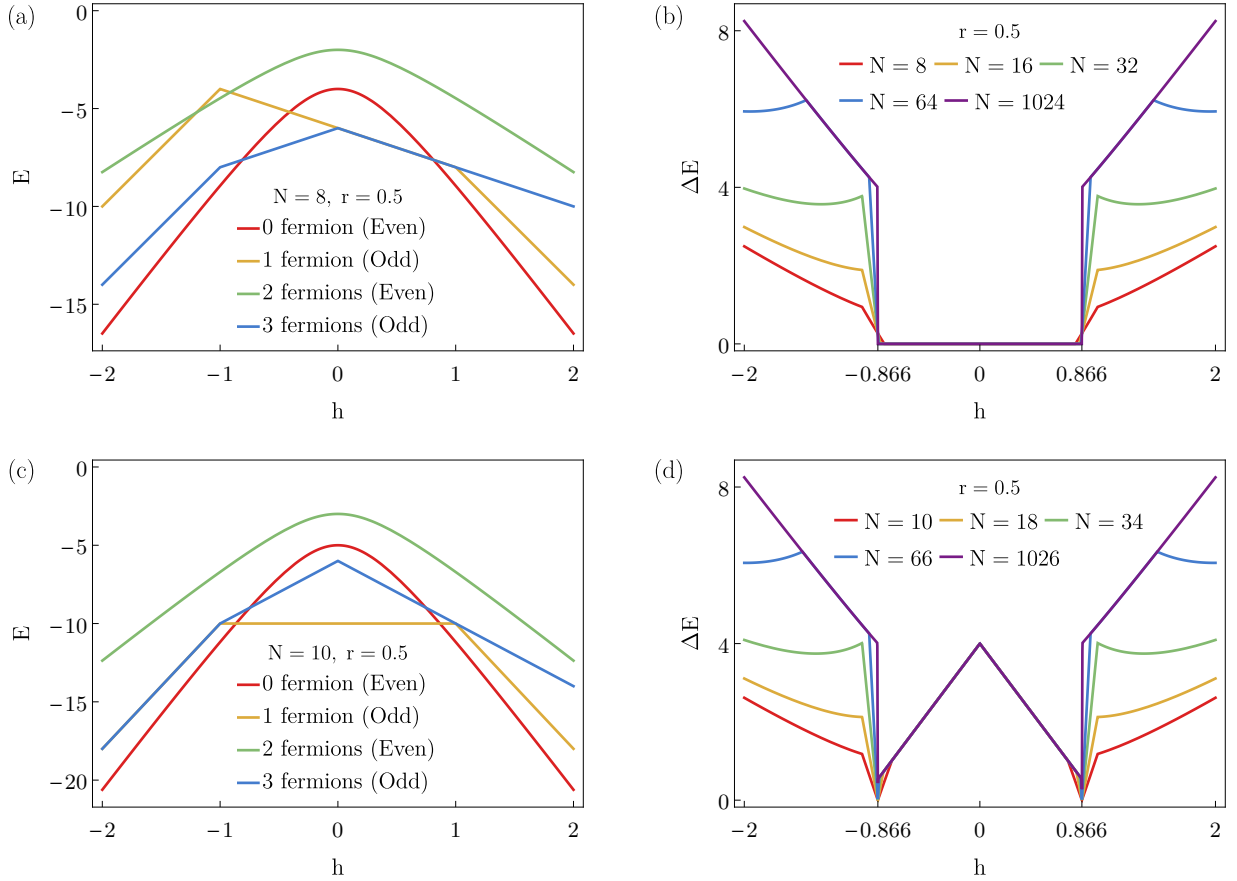


FIG. 6: Lowest few energy levels vs.  $h$  for the halfway XY model at  $r = 0.5$  with top (a):  $N = 8$ ; bottom (c):  $N = 10$ . This model shows that the ground state change from the odd to even sector at the transition. The right panel illustrates the energy gap vs.  $h$  for the halfway XY model at  $r = 0.5$ . Top (b):  $N = 4m$ ; bottom (d):  $N = 2(2m + 1)$ . There is clearly a difference between  $N = 4m$  and  $N = 2(2m + 1)$ . In the former, it is gapless in the range  $-0.86 \lesssim h \lesssim 0.86$ , but has a jump to a finite gap outside that range. On the other hand, in the latter case of  $N = 2(2m + 1)$ , inside the region  $-0.86 \lesssim h \lesssim 0.86$ , it is gapped, but the size of the gap has a jump at  $h \approx \pm 0.86$ . This suggests that the transition there is first-order, consistent with the level crossing, shown in (a) & (c).

$n = N/2 - 1$  (*halfway interaction*) exhibits different behavior from that of, e.g.,  $n = 0, 1$  and can prevent quantum phase transition in the halfway Ising limit ( $r = 1$ ) from appearing. This is a rather interesting result since except at this arbitrary point ( $n \neq N/2 - 1$ ), the XY model exhibits a quantum phase transition for each  $n$ -site interaction (See Fig. 5a). Moreover, we also discover a first-order phase transition in the XY model with halfway

interaction in the region of  $0 \leq r < 1$ . (Of course, in order to have the halfway interaction, the system size  $N$  must be even.) In this limit, the transition occurs at the Barouch-McCoy circle [53], namely  $r^2 + h^2 = 1$ . For example, in the case of  $r = 0.7$  the phase transition occurs at  $h_c = \sqrt{1 - 0.7^2} \approx 0.714$  as illustrated in Fig. 5(b). However, the halfway Ising model has no such transition. We note that for the standard XY model, the Barouch-McCoy circle represents only a crossover that divide the ferromagnetic phase into two regions. Here, for the halfway interaction, the circle represents a curve of first-order transition points.

First, let us define the parameters that give the XY model with  $n$ -site interaction

$$N^{(x)} = 1, \quad N^{(y)} = 1, \quad (76a)$$

$$J_l^{(x)} = \{(1+r)/2\}, \quad J_{l'}^{(y)} = \{(1-r)/2\}, \quad (76b)$$

$$n_l^{(x)} = \{n\}, \quad n_{l'}^{(y)} = \{n\}, \quad (76c)$$

yielding the corresponding Hamiltonian:

$$H_{XnY} = - \sum_{j=1}^N \left( \frac{1+r}{2} \sigma_{j-1}^x \sigma_j^z \dots \sigma_{j+n-1}^z \sigma_{j+n}^x + \frac{1-r}{2} \sigma_{j-1}^y \sigma_j^z \dots \sigma_{j+n-1}^z \sigma_{j+n}^y + h \sigma_j^z \right). \quad (77)$$

This Hamiltonian can be diagonalized by substituting above parameters into Eq. (16) and we obtain the following Bogoliubov solution where  $\phi_k^n \equiv \frac{2\pi}{N}(n+1)(k+b)$ :

$$\tan 2\theta_k^{(b)} = \frac{r \sin \phi_k^n}{h - \cos \phi_k^n}. \quad (78)$$

In the case of halfway interaction, we substitute  $n = N/2 - 1$  to simplify Bogoliubov solution for even ( $b = 1/2$ ) and odd sector ( $b = 0$ ):

$$\tan 2\theta_k^{(1/2)} = \frac{r \sin \left[ \pi \left( k + \frac{1}{2} \right) \right]}{h - \cos \left[ \pi \left( k + \frac{1}{2} \right) \right]} = \frac{(-1)^k r}{h}, \quad (79a)$$

$$\tan 2\theta_k^{(0)} = \frac{r \sin (\pi k)}{h - \cos (\pi k)} = 0, \quad (79b)$$

with following energy spectrum for even  $N$  and  $b = 1/2$ , and for odd  $N$  and  $b = 0$ :

$$\epsilon_k^{(b)} = \left\{ \begin{array}{ll} 2(h-1), & \text{for } k=0 \wedge b=0 \\ 2 \left[ h - \cos \left( \frac{\pi N}{2} \right) \right], & \text{for } k = \frac{N}{2} \wedge b=0 \\ 2 \left[ h - \cos \left( \frac{\pi N}{2} \right) \right], & \text{for } k = \frac{N-1}{2} \wedge b=1/2 \end{array} \right\} = 2\alpha_k^{(b)}, \quad (80)$$

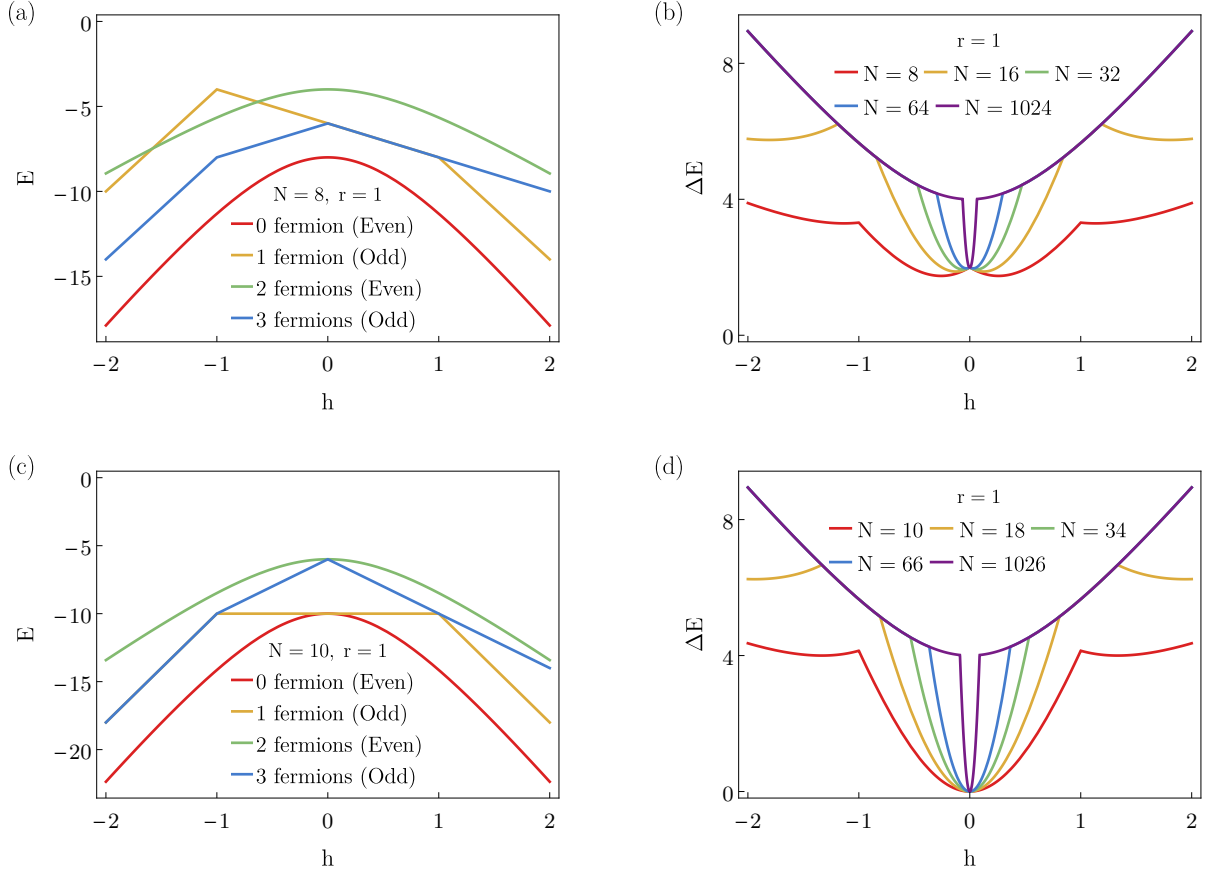


FIG. 7: The lowest two levels for even and odd sectors with top (a):  $N = 8$ ; bottom (c):  $N = 10$ , for the halfway Ising model at  $r = 1$ . We note that for the negative  $h$ , three-fermion occupation occurs as the lowest level in the odd sector, instead of one-fermion, which satisfy the inequality has shown in Eq. (21). The true ground state is constructed by the even sector ( $b = 1/2$ ) with no fermion. The right panel illustrates the energy gap between the ground state and the first excited state for halfway XY model as a function of  $h$  at  $r = 1$ . Top (b):  $N = 4m$ ; bottom (d):  $N = 2(2m + 1)$ . We see that as  $N$  becomes very large, the system becomes gapped at all  $h$ , except possible double degeneracy at  $h = 0$ . This shows that there is no phase transition in the thermodynamic limit.

or otherwise:

$$\epsilon_k^{(b)} = 2\sqrt{\left[h - \cos(\pi(b+k))\right]^2 + \left[r \sin(\pi(b+k))\right]^2} = \begin{cases} 2|h - (-1)^k|, & \text{for } b = 0, \\ 2\sqrt{h^2 + r^2}, & \text{for } b = 1/2. \end{cases} \quad (81)$$

To obtain the ground state and the first excited state, one should examine even and odd sectors carefully. This model shows vacua competition [39] similar to the standard XY

model, meaning the odd and even sector switch the roles of being the true ground state depending on  $h$ . This competition is lifted in the Ising limit where  $r = 1$  and the ground state is certainly constructed from the even sector ( $b = 1/2$ ) with no fermion, except when  $N = 2(2m + 1)$  and at  $h = 0$ , another degenerate ground state is from the odd sector with one fermion; see Fig. 7. In the case of  $r = 0.5$ , the switching happens around  $h \approx 0.86$ . The ground state becomes dominated by the odd sector in the range  $-0.87 \leq h < 0.87$ , but outside that range the ground state comes from the even sector ( $b = 0$ ) with zero-fermion occupation; see Fig. 6. In particular, for  $-0.87 \leq h < 0$  and with  $N = 4m$ , the lowest-energy level in the odd sector has three-fermion occupation instead of one fermion, as it is energetically favorable to occupy three fermions in the even sector rather than just one fermion. But in  $0 \leq h < 0.87$ , the lowest one-fermion and three-fermion states become degenerate. For  $N = 2(2m + 1)$  and  $-0.87 \leq h < 0.87$ , the lowest energy is dominated by the one-fermion state in the odd sector. This phenomena was anticipated earlier in Eq. (19-22). Using these equations we also calculated lowest energy for the odd/even sector and the true energy gap which can be seen in the Fig. 6. All of these suggest that there is a first-order phase transition for the halfway XY model with  $0 \leq r < 1$ , as the transition is due to a level crossing. However, for  $r = 1$ , the halfway Ising model does not have a phase transition.

There is an interesting picture that emerges. In the standard XY model in a transverse field, there is a crossover curve, the so-called Barouch-McCoy circle, given by  $r^2 + h^2 = 1$  [53]. The crossover curve divides the ferromagnetic phase into two regions: (i) inside the arc, the spin-spin correlation functions display oscillatory behavior, (ii) outside the arc, the correlation functions has no oscillatory behavior. On the arc, the ground state is essentially a product state, also detected by zero geometric entanglement previously in Ref. [21]. Here for the halfway XY model, the crossover arc,  $r^2 + h^2 = 1$  is promoted to a first-order transition curve, due to the mediated long-range Z string of a specific length  $n = N/2 - 1$ . Thus the transition field  $h$  for  $r = 0.5$  is  $h_c(r = 0.5) = \sqrt{1 - 0.5^2} \approx 0.886$ , agreeing with our calculations of the energy gap in Fig. 6. This works for other value of  $0 \leq r < 1$  as well, see Fig. 5(b) for  $r = 0.7$  case. But the  $r = 1$  halfway Ising model does not have a transition as shown in Fig. 7.

As the transition in the halfway XY model is first-order, one expects that the entanglement will have a discontinuity at the transition, as it is caused by a level crossing. In this

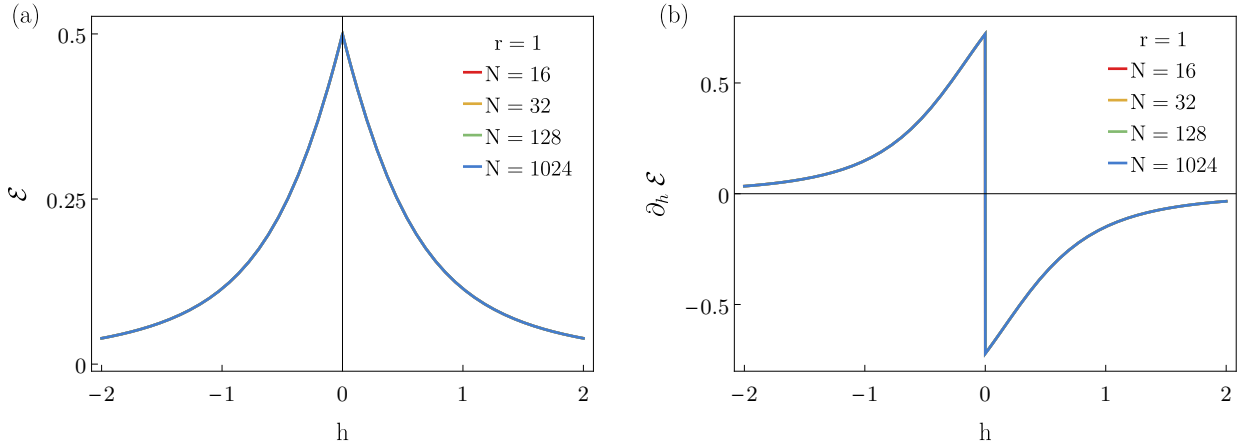


FIG. 8: (a) The figure shows the entanglement per site at  $r = 1$  with increasing system sizes  $N = 16, 32, 128, 1024$ , all of which collapse on the same line. (b) The cusp of the entanglement in (c) gives rise to a jump in the entanglement derivative.

case, the ground state in the range  $-\sqrt{1-r^2} \leq h \leq \sqrt{1-r^2}$  involves the even sector with either one or three fermions. One could calculate the ground-state overlap with product states. But we will not proceed with that here. For  $r = 1$  halfway Ising model, as well as other Ising models with  $n$ -site interaction, the ground-state wavefunction comes from the even sector without a fermion, and for that the overlap has been calculated in Sec. III, and hence the geometric entanglement (per site and per block of two sites) is readily available upon simple parameter optimization. As shown in Fig. 8, the entanglement develops a cusp behavior at  $h = 0$  and giving rise to a jump in the derivative. However, this ‘weak’ singularity is a result that the entanglement is symmetric w.r.t.  $h = 0$ , but it immediately decreases as soon as  $h$  deviates from 0 (i.e. with a non-zero slope). As shown in Ref. [44], at  $h = 0$ , the state there is the generalized cluster state, which exhibits the same geometric entanglement as the cluster state, and is expected to display the infinite localizable entanglement length [54]. Even though there is no true phase transition in the usual statistical mechanics, but there is one peculiar transition there proposed by Verstraete, Martin-Delgado and Cirac [54] in that the localizable entanglement length is infinite. This kind of transition was shown to be detectable by the geometric entanglement, displaying the weak singularity, such as the cusp [51].

### C. GHZ-Cluster model

In this part, we study the ground-state energy of the GHZ-Cluster model, which was introduced by Wolf et al. [28], and examine the quantum phase transition on the phase diagram, utilizing the geometric entanglement and the energy gap. We consider a local Hamiltonian with three-site interaction constructed by the following matrix product state as its ground state,

$$A_0 = \begin{pmatrix} 0 & 0 \\ 1 & 1 \end{pmatrix}, \quad A_1 = \begin{pmatrix} 1 & g \\ 0 & 0 \end{pmatrix}, \quad (82)$$

and the corresponding Hamiltonian possessing  $\mathbb{Z}_2$  symmetry was constructed by Wolf et al. [28] and reads:

$$H = \sum_{j=1}^N \left( 2(g^2 - 1)\sigma_{j-1}^z \sigma_j^z + (g - 1)^2 \sigma_{j-1}^z \sigma_j^x \sigma_{j+1}^z - (1 + g)^2 \sigma_j^x \right). \quad (83)$$

The QPT in the model is peculiar as the ground-state energy is analytic for all range of the parameter  $g$ , even though the correlation length diverges at the critical point.

To utilize our parameterization for the model, first we rotate the Hamiltonian around the  $y$  axis such that  $\sigma_x \rightarrow \sigma_z$ . Then we choose  $N^{(x)} = 2$  and a list of  $J_l^{(x)}$ , as we need two  $X$  blocks and  $N^{(y)} = 0$  to eliminate  $Y$  block. We note that one can assign the value for  $h$  in terms of  $g$  to generate the desired Hamiltonian. Here we give the resulting parameters that give the equivalent cluster-GHZ model:

$$h = (1 + g)^2, \quad (84a)$$

$$N^{(x)} = 2, \quad N^{(y)} = 0, \quad (84b)$$

$$J_l^{(x)} = \{-2(g^2 - 1), -(g - 1)^2\}, \quad J_l^{(y)} = \{0\}, \quad (84c)$$

$$n_l^{(x)} = \{0, 1\}, \quad n_l^{(y)} = \{0\}, \quad (84d)$$

and we arrive at the following equivalent Hamiltonian:

$$H = - \sum_{j=1}^N \left( -2(g^2 - 1)\sigma_{j-1}^x \sigma_j^x - (g - 1)^2 \sigma_{j-1}^x \sigma_j^z \sigma_{j+1}^x + (1 + g)^2 \sigma_j^z \right). \quad (85)$$

By substituting above parameters into Eq. (16) we obtain the diagonalized Hamiltonian with the following Bogoliubov solution where  $\varphi_k^{(b)} \equiv \frac{2\pi(b+m)}{N}$ ,

$$\tan 2\theta_k^{(b)} = - \frac{2(g - 1) \sin \varphi_k^{(b)} [(g - 1) \cos \varphi_k^{(b)} + g + 1]}{2(g^2 - 1) \cos \varphi_k^{(b)} + (g - 1)^2 \cos 2\varphi_k^{(b)} + (g + 1)^2}. \quad (86)$$

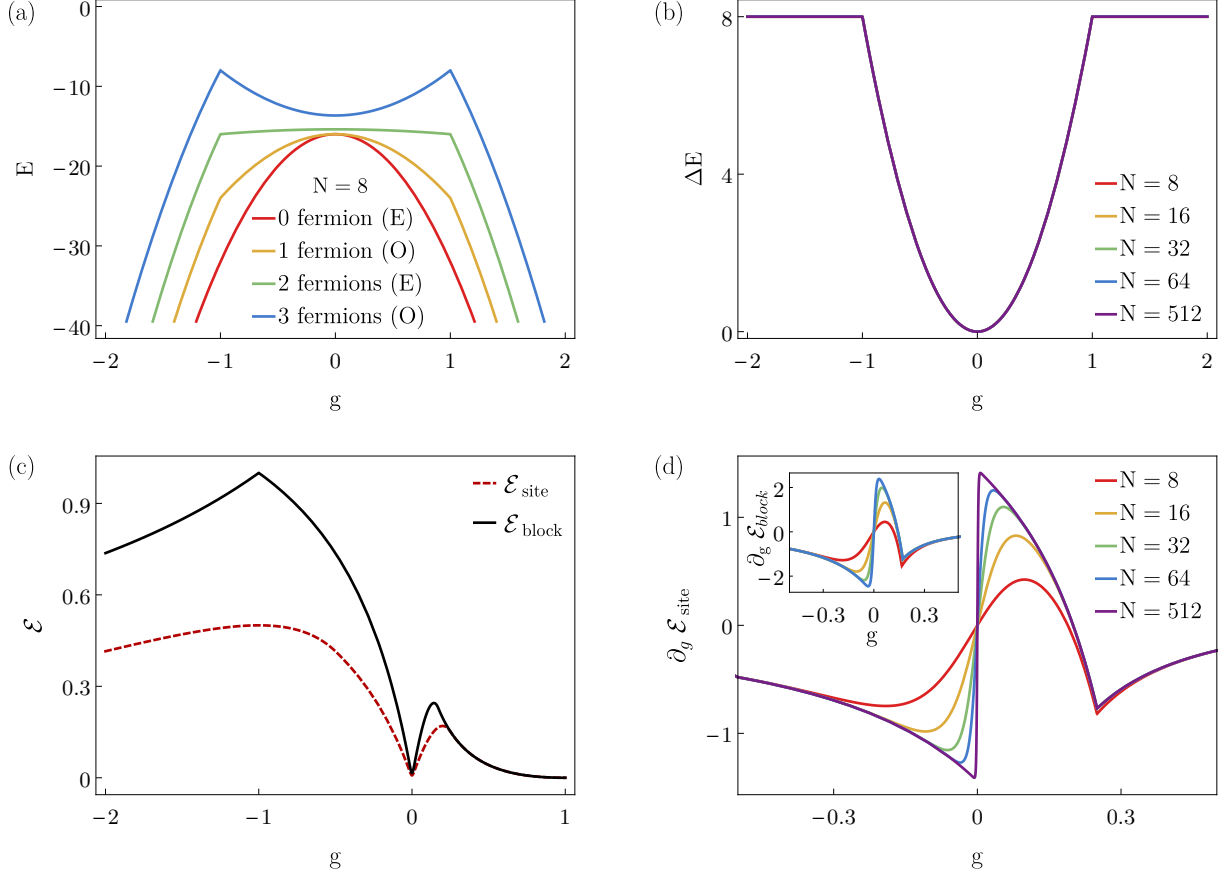


FIG. 9: (a) The lowest few energy levels for even and odd sector in GHZ-cluster model, with  $N = 8$ , as a function of  $g$ . We use E. & O. to imply Even and Odd sector respectively. (b) The energy gap for increasing system sizes ( $N = 8, 16, 32, 64, 512$ ), interesting, are the same. As constructed in Ref. [26], the ground-state energy displays no singularity at the QPT ( $g = 0$ ). (c) The transition can be detected by the behavior of entanglement. The figure shows geometric entanglement per site (red, dashed) and per block (black, solid) for GHZ-Cluster state where  $N = 128$ . (d) Derivative of the entanglement per site and per block (inset) close to the critical point at  $g = 0$ , where  $N = 8, 16, 32, 64, 512$  is used (bottom to top).

The exact energy spectrum can be obtained by utilizing Eq. (14) & (17-20). The eigenvalues in the case of even  $N$  for odd sector ( $b = 0$ , periodic boundary conditions) and even sector

( $b = 1/2$ , antiperiodic boundary conditions) are as follows,

$$\epsilon_k^{(b)} = \begin{cases} 8g^2, & \text{for } k = 0 \wedge b = 0 \\ 8, & \text{for } k = \frac{N}{2} \wedge b = 0 \\ 8, & \text{for } k = \frac{N-1}{2} \wedge b = 1/2 \end{cases} = 2\alpha_k^{(b)}, \quad (87)$$

or otherwise:

$$\epsilon_k^{(b)} = 4 \left[ 1 + g^2 + (g^2 - 1) \cos \left( \frac{2\pi(k+b)}{N} \right) \right]. \quad (88)$$

The model exhibits quantum phase transition at  $g_c = 0$ , and the ground state there is the Greenberger-Horne-Zeilinger (GHZ) state. At  $g = 1$ , the Hamiltonian is proportional to  $\sum_j \sigma_j^z$  where all spins are in the  $z$ -direction; this is a paramagnetic phase. At  $g = -1$  the ground state is a cluster state (disordered phase), and the Hamiltonian has a  $Z_2 \times Z_2$  symmetry. The cluster state is a representative nontrivial  $Z_2 \times Z_2$  SPT state. However, the model only has  $Z_2$  symmetry at  $g \neq -1$ . Here we also obtain the exact energy spectrum for this model using Eq. (17-30) and analyze how the ground and first excited states are composed of by examining odd/even sector and number of fermions occupation. If we restrict ourselves to the region  $-2 < g < 2$ , we find that the ground state comes from the even sector ( $b = 1/2$ ) with no fermions and the first excited state is constructed from the odd sector ( $b = 0$ ) with one-fermion occupation. The ground state in the model does not have three-fermion occupation in any finite  $g$ , see Fig. 9(a). We point that for any system size  $N$ (even), the energy gap is equal to  $\Delta E = 8g^2$  in the regime of  $-1 < g < 1$ ; otherwise outside that range the energy gap is always  $\Delta E = 8$ , regardless of the system size. As already shown by construction in Ref. [28] and confirmed here by calculation, the ground-state energy displays no singularity at the critical point  $g = 0$ ; see Fig. 9(b). It is a peculiar type of quantum phase transition, as emphasized in Ref. [28].

Figure 9(c) shows the global entanglement upon using the solution which we derived in the previous section. It contains the global entanglement per site (red, dashed) and per block (black, L=2). One can examine the derivative of the entanglement [27] to see the divergence near the critical point. As shown in Fig. 9(d), the quantum phase transition is detected at the GHZ point ( $g = 0$ ) by the behavior of entanglement. We note that at  $g = -1$ , the entanglement per block shows a cusp behavior, but there is no true phase transition there. However, there is a transition there in the sense of infinite localizable entanglement length [54]. As remarked earlier, this kind of transition was shown to be detectable by the

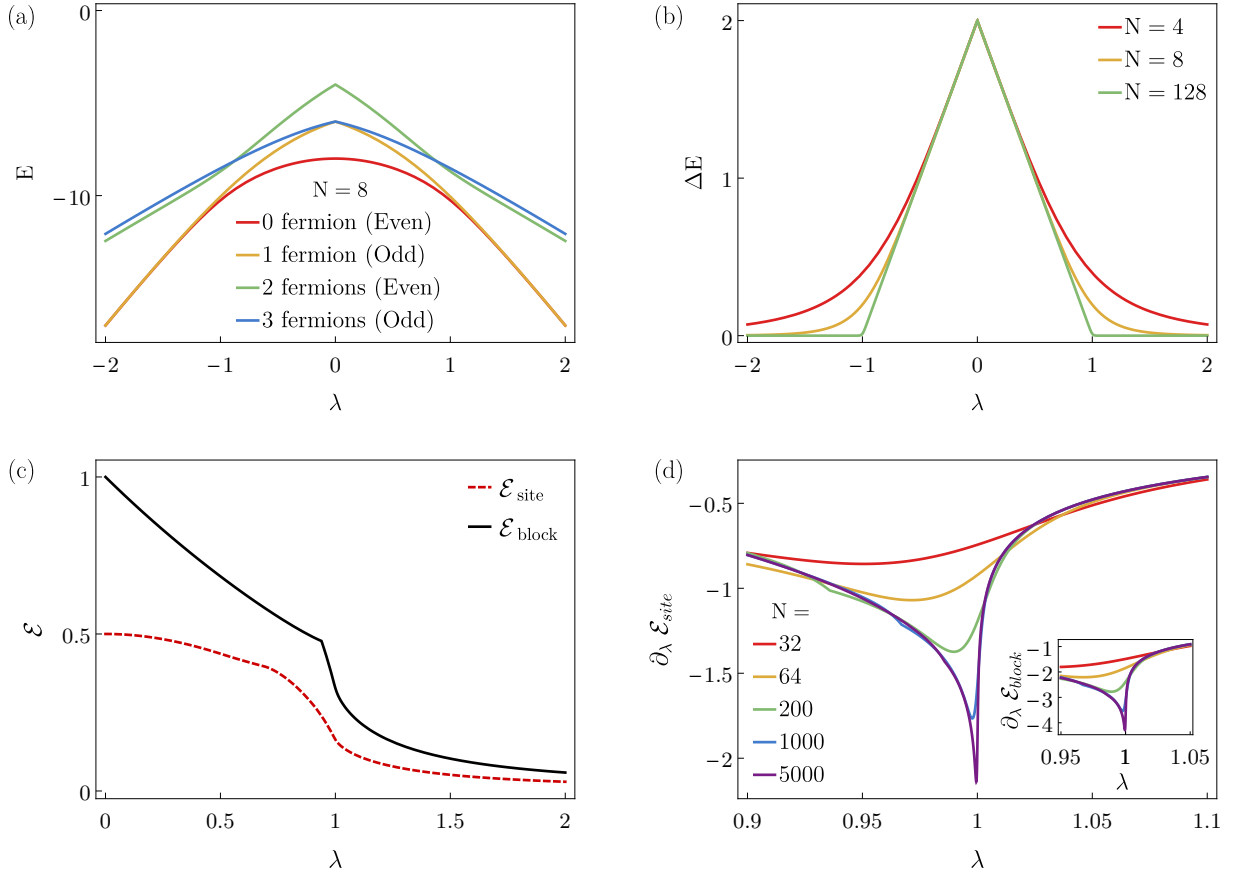


FIG. 10: (a) Lowest few energy levels vs.  $\lambda$  for the SPT-AFM model with  $N = 8$ . (b) The energy gap between the ground state and the first excited state as a function of  $\lambda$ . The ground state is degenerate for  $\lambda \geq 1$  in the thermodynamic limit and the energy gap becomes  $\Delta E = 2(1 - |\lambda|)\theta(1 - |\lambda|)$ . Thus the singularity at  $\lambda = 1$  signals a quantum phase transition. (c) Geometric entanglement per site (red, dashed) and per block (black) for SPT-Antiferromagnetic chain where  $N = 200$ ; (d) Derivative of the entanglement per site (the inset shows that for per block) where  $N=32, 64, 200, 1000, 5000$  (from top to bottom).

geometric entanglement in the form of weak singularity, such as the cusp [51].

#### D. SPT-Antiferromagnetic transition

At the last example, we examine a particular quantum phase transition [55, 56] between a symmetry protected topological order and an antiferromagnetic phase by using the same method we derived. In order to construct the Hamiltonian, we choose one  $X$  and one  $Y$  block

and set  $h = 0$  to eliminate the transverse-field term. Parameters of the model considered are shown as follows:

$$h = 0, \quad (89a)$$

$$N^{(x)} = 1, \quad N^{(y)} = 1, \quad (89b)$$

$$J_l^{(x)} = \{1\}, \quad J_{l'}^{(y)} = \{-\lambda\}, \quad (89c)$$

$$n_l^{(x)} = \{1\}, \quad n_{l'}^{(y)} = \{0\}, \quad (89d)$$

which give the following Hamiltonian:

$$H = - \left( \sum_{j=1}^N \sigma_{j-1}^x \sigma_j^z \sigma_{j+1}^x - \lambda \sum_{j=1}^N \sigma_{j-1}^y \sigma_j^y \right). \quad (90)$$

By substituting above parameters into Eq. (16) we obtain the diagonalized Hamiltonian with the following Bogoliubov solution:

$$\tan 2\theta_k^{(b)} = \frac{\lambda \sin\left(\frac{2\pi(b+k)}{N}\right) + \sin\left(\frac{4\pi(b+k)}{N}\right)}{\lambda \cos\left(\frac{2\pi(b+k)}{N}\right) - \cos\left(\frac{4\pi(b+k)}{N}\right)}. \quad (91)$$

The exact energy spectrum can be obtained by utilizing Eq. (14) & (17-20). The eigenvalues in the case of even  $N$  for odd sector ( $b = 0$ , periodic boundary conditions) and even sector ( $b = 1/2$ , antiperiodic boundary conditions) are as follows

$$\epsilon_k^{(b)} = \left\{ \begin{array}{ll} 2(1 - \lambda), & \text{for } k = 0 \wedge b = 0 \\ 2(1 + \lambda), & \text{for } k = \frac{N}{2} \wedge b = 0 \\ 2(1 + \lambda), & \text{for } k = \frac{N-1}{2} \wedge b = 1/2 \end{array} \right\} = 2\alpha_k^{(b)}, \quad (92)$$

or otherwise:

$$\epsilon_k^{(b)} = 2\sqrt{1 + \lambda^2 - 2\lambda \cos\left(\frac{6\pi}{N}(k + b)\right)}. \quad (93)$$

The even sector ( $b = 1/2$ ) with no fermions corresponds to the ground state energy for finite system size  $N$ (even) whereas the first excited state comes from the odd sector ( $b = 0$ ) with one fermion occupation Fig. 10(a). The energy gap in this case can be obtained by calculating  $\Delta E = E_{b=0} - E_{b=1/2}$  which is approximately  $2(1 - |\lambda|)$  in the region  $-1/2 < \lambda < 1/2$  for small system size ( $N$ ). In the thermodynamic limit ( $N \rightarrow \infty$ ) the energy gap becomes  $\Delta E = (1 - |\lambda|) [1 + \text{sgn}(1 - |\lambda|)]$  for all regions  $-\infty < \lambda < \infty$ . The critical point  $\lambda = 1$ , can be deduced from the energy gap in the thermodynamic limit; see Fig. 10(b).

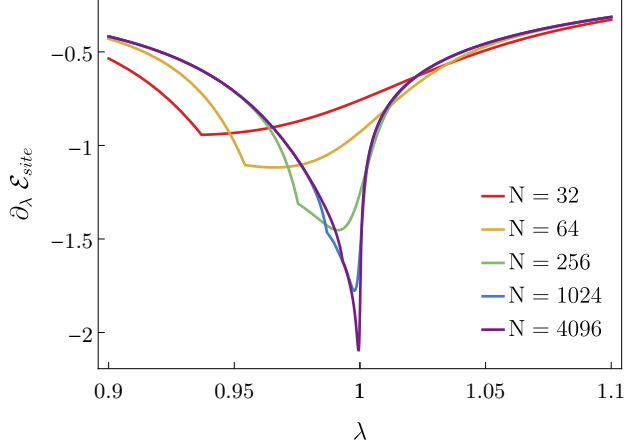


FIG. 11: Derivative of the entanglement per site where  $N=32, 64, 128, 1024, 4096$  (from top to bottom) for SPT-Antiferromagnetic chain with halfway interaction.

We also calculated site & block entanglement, shown in Fig. 10, as well as the exact solution of the energy spectrum. As can be seen from Fig. 10(d), the derivative of the entanglement per site has singularity at  $\lambda = 1$  where quantum phase transition occurs between the cluster and the antiferromagnetic phase. We note that as the antiferromagnetic phase is involved in the model, in order to compute entanglement per site, we use the closest product state of the form  $|\Phi\rangle = \prod_i |\phi^{[2i-1, 2i]}\rangle$  with  $|\phi^{[2i-1, 2i]}\rangle = (\alpha|\uparrow\rangle + \beta|\downarrow\rangle)(\gamma|\uparrow\rangle + \delta|\downarrow\rangle)$ . The entanglement derivative w.r.t.  $\lambda$  clearly also shows a divergence at  $\lambda = 1$  as  $N$  increases. This is a QPT separating an SPT phase and an antiferromagnetic ordered phase. The representative state in the SPT phase is the 1D cluster state [57, 58]. We remark that there is a weak singularity in the entanglement per block around  $\lambda \approx 0.94$ , but we cannot identify the state there and do not know the nature of this singularity. It might be a transition in localizable entanglement, but that requires further investigation.

Beyond reproducing results by Son et al. [29], we also examine a slight variation of the model, where, instead of  $XZX$ , the *halfway interaction* for  $X$  blocks is considered, as shown in the following Hamiltonian:

$$H = - \left( \sum_{j=1}^N \sigma_{j-1}^x \sigma_j^z \cdots \sigma_{j+(N/2)-2}^z \sigma_{j+(N/2)-1}^x - \lambda \sum_{j=1}^N \sigma_{j-1}^y \sigma_j^y \right). \quad (94)$$

The parameters for this model can be defined as follows:

$$h = 0, \tag{95a}$$

$$N^{(x)} = 1, \quad N^{(y)} = 1, \tag{95b}$$

$$J_i^{(x)} = \{1\}, \quad J_{i'}^{(y)} = \{-\lambda\}, \tag{95c}$$

$$n_i^{(x)} = \{N/2 - 1\}, \quad n_{i'}^{(y)} = \{0\}. \tag{95d}$$

The model can be exactly diagonalized with the following Bogoliubov solution:

$$\tan 2\theta_k^{(b)} = \frac{\lambda \sin\left(\frac{2\pi(b+k)}{N}\right) + \sin(\pi(b+k))}{\lambda \cos\left(\frac{2\pi(b+k)}{N}\right) - \cos(\pi(b+k))}. \tag{96}$$

The geometric entanglement still gives singularity at the critical point  $\lambda = 1$ , where quantum phase transition occurs (See Fig. 11). This is in contrast to the halfway Ising model with a transverse field, where somehow the halfway interaction prevents the QPT in the model, as discussed in Sec. IV B.

## V. CONCLUSION

In this work, we introduced a convenient parameterization for a general class of exactly solvable spin chains, which we called the cluster-XY models. We reviewed the procedure to diagonalize these spin chains and obtained the energy spectrum, the ground-state energy, the ground-state wavefunctions, and the energy gap. We illustrated subtlety in determining the true ground state, as it can come from two different sectors, with different number of fermions. The quantum phase transitions can be studied from the energy gap in the thermodynamic limit. Furthermore, we employed the geometric measure of entanglement per site/block for quantifying entanglement in the multipartite system. We presented detailed calculations for the overlap of the ground states with two different types of product states. From this, we examined global entanglement near the quantum critical point and investigated the quantum phase transition in several illustrative models, that include the three-site interacting XY model, the XY model with halfway interaction, the GHZ-cluster model, and the SPT-AFM models (and a variation of the last model).

Among the above models, the XzY model possesses a  $Z_2 \times Z_2$  symmetry and exhibits transitions from nontrivial SPT phase to a trivial paramagnetic phase. Moreover, the halfway

XY model exhibits a first-order transition across the Barouch-McCoy circle, on which it is only a crossover in the standard XY model. However, the halfway Ising model has no such transition. The GHZ-cluster model was constructed in Ref. [26] to exhibit a QPT but without singularity in ground-state energy. Geometric entanglement is able to detect such QPT [27]. The SPT-AFM model is an interesting example that has a transition between a symmetry-protected topological phase and a symmetry-breaking phase, constructed by Son et al. [29] and we not only reproduced the entanglement per site but also presented the entanglement per block. Both quantities display singularity near the critical point. Furthermore, we also studied a peculiar variation, where the cluster interaction  $XZX$  is replaced by a halfway interaction. In contrast to the halfway Ising model, this halfway SPT-AFM model exhibits a QPT. Our study on arbitrary  $n$ -site XY model generalizes previous study on the XY model via the geometric entanglement [21]. The examples we gave demonstrate the usefulness of our general results on entanglement in the family of the generalized XY-cluster models.

Regarding the entanglement per block, we were able to obtain analytic results for a block of two sites. The two-site state can be generally entangled, but can also be set to be a product state. The latter is useful for the geometric entanglement per site in the case of antiferromagnetic ground states, as the globally closest product state cannot be translationally invariant. Even though numerically one can compute per block of any number of sites, it would be interesting to derive analytically the overlap with block product state with any number of sites in a block. Then the entanglement under RG can be studied in further details. We leave it for future exploration.

### **Acknowledgments**

This work was supported by National Science Foundation via Grants No. PHY 1620252 and No. PHY 1314748. A. Deger hereby acknowledges Fulbright scholarship, granted by the U.S. Department of State's Bureau of Educational and Cultural Affairs, to fund the author during this research in Stony Brook University. Some of the results are based on his

master's thesis submitted to the Graduate School at Stony Brook University in 2016 [59].

---

- [1] A. Einstein, B. Podolsky, and N. Rosen, *Phys. Rev.* **47**, 777 (1935).
- [2] J. S. Bell, *On the einstein podolsky rosen paradox* (1964).
- [3] J. F. Clauser, M. A. Horne, A. Shimony, and R. A. Holt, *Phys. Rev. Lett.* **23**, 880 (1969).
- [4] S. J. Freedman and J. F. Clauser, *Phys. Rev. Lett.* **28**, 938 (1972).
- [5] A. Aspect, P. Grangier, and G. Roger, *Phys. Rev. Lett.* **47**, 460 (1981).
- [6] W. Tittel, J. Brendel, B. Gisin, T. Herzog, H. Zbinden, and N. Gisin, *Phys. Rev. A* **57**, 3229 (1998).
- [7] G. Weihs, T. Jennewein, C. Simon, H. Weinfurter, and A. Zeilinger, *Phys. Rev. Lett.* **81**, 5039 (1998).
- [8] M. Nielsen and I. L. Chuang, *Quantum computation and quantum information* (2000).
- [9] C. H. Bennett, G. Brassard, C. Crépeau, R. Jozsa, A. Peres, and W. K. Wootters, *Phys. Rev. Lett.* **70**, 1895 (1993).
- [10] P. W. Shor, in *Foundations of Computer Science, 1994 Proceedings., 35th Annual Symposium on* (IEEE, 1994), pp. 124–134.
- [11] L. K. Grover, in *Proceedings of the twenty-eighth annual ACM symposium on Theory of computing* (ACM, 1996), pp. 212–219.
- [12] A. K. Ekert, *Phys. Rev. Lett.* **67**, 661 (1991).
- [13] J. Maldacena and L. Susskind, *Fortschr. Phys.* **61**, 781 (2013).
- [14] J. Steinhauer, *Nat. Phys.* **12**, 959 (2016).
- [15] L. Amico, R. Fazio, A. Osterloh, and V. Vedral, *Rev. Mod. Phys.* **80**, 517 (2008).
- [16] I. Peschel, *Braz. J. Phys.* **42**, 267 (2012).
- [17] V. Vedral, M. B. Plenio, M. A. Rippin, and P. L. Knight, *Phys. Rev. Lett.* **78**, 2275 (1997), 9702027.
- [18] W. K. Wootters, *Phys. Rev. Lett.* **80**, 2245 (1998).
- [19] H. Barnum and N. Linden, *J. Phys. A: Math. Theor.* **34**, 6787 (2001), 0103155.
- [20] T.-C. Wei and P. M. Goldbart, *Phys. Rev. A* **68**, 042307 (2003).
- [21] T.-C. Wei, D. Das, S. Mukhopadhyay, S. Vishveshwara, and P. M. Goldbart, *Phys. Rev. A* **71**, 060305 (2005).

- [22] S. Sachdev, *Quantum Phase Transitions* (John Wiley & Sons, Ltd, 2007).
- [23] T. J. Osborne and M. a. Nielsen, *Quantum Inf. Process.* **1**, 45 (2002).
- [24] L. Amico, F. Baroni, A. Fubini, D. Patanè, V. Tognetti, and P. Verrucchi, *Phys. Rev. A* **74**, 022322 (2006).
- [25] A. Osterloh, L. Amico, G. Falci, and R. Fazio, *Nature* **416**, 608 (2002).
- [26] F. Verstraete, J. I. Cirac, J. I. Latorre, E. Rico, and M. M. Wolf, *Phys. Rev. Lett.* **94**, 140601 (2005).
- [27] T.-C. Wei, *Phys. Rev. A* **81**, 062313 (2010).
- [28] M. M. Wolf, G. Ortiz, F. Verstraete, and J. I. Cirac, *Phys. Rev. Lett.* **97**, 110403 (2006).
- [29] W. Son, L. Amico, R. Fazio, A. Hamma, S. Pascazio, and V. Vedral, *EPL* **95**, 50001 (2011).
- [30] S. Montes and A. Hamma, *Phys. Rev. E* **86**, 021101 (2012).
- [31] E. Lieb, T. Schultz, and D. Mattis, *Ann. Phys.* **16**, 407 (1961).
- [32] B. M. McCoy, *Phys. Rev.* **173**, 531 (1968).
- [33] E. Barouch, B. M. McCoy, and M. Dresden, *Phys. Rev. A* **2**, 1075 (1970).
- [34] F. Verstraete, M. Popp, and J. I. Cirac, *Phys. Rev. Lett.* **92**, 027901 (2004).
- [35] J. K. Pachos and M. B. Plenio, *Phys. Rev. Lett.* **93**, 1 (2004), 0401106.
- [36] P. Lou, W. C. Wu, and M. C. Chang, *Phys. Rev. B* **70**, 064405 (2004).
- [37] V. Derzhko, O. Derzhko, and J. Richter, *Phys. Rev. B* **83**, 174428 (2011), 1012.2058.
- [38] I. Titvinidze and G. I. Japaridze, *Eur. Phys. J. B* **32**, 383 (2003), 0211380v3.
- [39] A. De Pasquale and P. Facchi, *Phys. Rev. A* **80**, 1 (2009), 0808.1478.
- [40] H. Primakoff and T. Holstein, *Phys. Rev.* **55**, 1218 (1939).
- [41] M. Azzouz, *Phys. Rev. B* **48**, 6136 (1993).
- [42] J. Bardeen, L. N. Cooper, and J. R. Schrieffer, *Phys. Rev.* **108**, 1175 (1957).
- [43] M. Suzuki, *Progress of Theoretical Physics* **46**, 1337 (1971).
- [44] V. Lahtinen and E. Ardonne, *Phys. Rev. Lett.* **115**, 237203 (2015).
- [45] G. Vidal, J. I. Latorre, E. Rico, and A. Kitaev, *Phys. Rev. Lett.* **90**, 227902 (2003).
- [46] P. Calabrese and J. Cardy, *J. Stat. Mech: Theory Exp.* **2004**, P06002 (2004).
- [47] M.-C. Chung and I. Peschel, *Phys. Rev. B* **64**, 064412 (2001).
- [48] V. E. Korepin, *Phys. Rev. Lett.* **92**, 096402 (2004).
- [49] R. Orus, S. Dusuel, and J. Vidal, *Phys. Rev. Lett.* **101**, 025701 (2008).
- [50] R. Orus, *Phys. Rev. Lett.* **100**, 130502 (2008).

- [51] R. Orus and T.-C. Wei, *Phys. Rev. B* **82**, 155120 (2010).
- [52] T.-C. Wei, S. Vishveshwara, and P. M. Goldbart, *Quantum Inf. & Comp.* **11**, 326 (2011).
- [53] E. Barouch and B. M. McCoy, *Phys. Rev. A* **3**, 786 (1971).
- [54] F. Verstraete, M. A. Martín-Delgado, and J. I. Cirac, *Phys. Rev. Lett.* **92**, 087201 (2004).
- [55] Z.-C. Gu and X.-G. Wen, *Phys. Rev. B* **80**, 155131 (2009).
- [56] F. Pollmann, E. Berg, A. M. Turner, and M. Oshikawa, *Phys. Rev. B* **85**, 075125 (2012).
- [57] R. Raussendorf and H. J. Briegel, *Phys. Rev. Lett.* **86**, 5188 (2001).
- [58] D. V. Else, I. Schwarz, S. D. Bartlett, and A. C. Doherty, *Phys. Rev. Lett.* **108**, 240505 (2012).
- [59] A. Deger, Master's thesis, State University of New York at Stony Brook (2016).